Engineering Structures 338 (2025) 120589

Contents lists available at ScienceDirect

Engineering Structures

journal homepage: www.elsevier.com/locate/engstruct

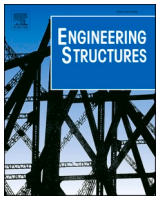

Fire-induced spalling in hybrid polyethylene fiber-reinforced engineered cementitious composite panels

S. Rawat [a,b], Lihai Zhang [c], Y.X. Zhang [a,*]

[a] Centre for Advanced Manufacturing Technology, School of Engineering, Design and Built Environment, Western Sydney University, NSW 2751, Australia
[b] School of Civil and Environmental Engineering, University of Technology Sydney (UTS), Sydney, NSW 2007, Australia
[c] School of Infrastructure Engineering, The University of Melbourne, VIC 3010, Australia

ARTICLE INFO

Keywords:
Engineered cementitious composite (ECC)
Fire resistance
Hybrid fibre
Polyethylene fibre
Spalling

ABSTRACT

Polyethylene (PE) fibre-reinforced engineered cementitious composites (ECC) offer high ductility and durability, however concerns over fire performance, particularly spalling resistance, continue to limit their adoption. This study evaluates single and hybrid PE fibre-reinforced ECC with high-volume slag and MgO under fire exposure, examining spalling resistance at both material and structural scales. Key test parameters include PE fibre length (9, 12, 18 mm), fibre type (single or hybrid with polypropylene (PP) and basalt fibre), and panel size (300 ×300 mm, 200 ×200 mm, 100 ×100 mm) and thickness (20, 50 mm). A novel 1-directional (1-D) spalling test is also developed and compared with a traditional 3-directional (3-D) furnace test. Material-scale tests showed that replacing 12 mm, 0.75 % PE fibre with basalt improved strength retention at elevated temperatures by approximately 5–7 %, achieving a total retention of 37–40 %. However, large-scale tests revealed poor spalling resistance with this mix as full-thickness spalling occurred in 300 × 300 × 50 mm panels. Spalling resistance improved with longer PE fibres (18 mm) or the addition of PP fibres, with a hybrid mix (12 mm 0.3 % PP, 1.25 % PE, 0.75 % basalt) demonstrating superior performance. Further analysis indicated that fibre melting may not be the primary mechanism for spalling resistance; rather, fibre distribution and bonding with the matrix are critical for forming an effective network for vapour pressure dissipation.

1. Introduction

Fire poses a significant risk to engineering structures such as tall buildings and is one of the most common threats to life and property [1]. One particularly dangerous phenomenon is 'fire-induced spalling', where concrete fragments detach from the heated surface, potentially leading to structural failure. Spalling occurs through three primary mechanisms: (a) *thermo-hygral spalling* (200–400°C), caused by rapid water vaporisation and thermal gradients; (b) *thermo-mechanical spalling* (400–700°C), resulting from thermal stresses and external loads; and (c) *thermo-chemical spalling* (>700°C), driven by the decomposition of the cementitious matrix [2–4]. Thermo-hygral and thermo-chemical spalling are particularly severe in materials with dense microstructures and high cementitious content.

Engineered cementitious composite (ECC) is one such material, known for its superior durability and strength, and has been utilized in diverse applications such as tunnels, high-rise building and retrofitting [5]. Among various ECCs, polyethylene (PE) fibre-reinforced ECC (PE-ECC) has demonstrated outstanding tensile strain hardening and ductility compared to mixes reinforced with polyvinyl alcohol, steel, or basalt fibres. Despite its advantages, the fire performance of PE-ECC remains a concern [3]. Polymer fibres, such as PE, are expected to mitigate thermo-hygral spalling by forming melted fibre channels that relieve pore pressure. However, severe explosive spalling has been observed even at high fibre volumes (1.3–1.8 %) [6–10]. For instance, Liu and Tan [6] observed spalling in ECC specimens reinforced with 1.3 % PE fibre. Similarly, Zhang et al. [7] noted spalling in ECC mixes with 1.5 % PE fibre, and recently, Zhang et al. [8] reported that even a fibre volume of 1.8 % does not prevent spalling. The studies suggested that the severity of spalling in these cases may be related to factors like large molecular size and low coefficient of thermal expansion of PE fibres. Although the addition of polypropylene (PP) or steel fibres and improving the cementitious matrix have enhanced material-scale spalling resistance [6,7,11,12], it remains unclear whether these modifications translate to improved performance in large-scale specimens.

Another critical gap in the literature is the lack of structural (large)

* Corresponding author.
E-mail addresses: sanket.rawat@uts.edu.au (S. Rawat), lihzhang@unimelb.edu.au (L. Zhang), sarah.zhang@uts.edu.au (Y.X. Zhang).

https://doi.org/10.1016/j.engstruct.2025.120589
Received 29 September 2024; Received in revised form 5 April 2025; Accepted 15 May 2025
Available online 24 May 2025

Table 1
Matrix constituents for the present study.

Binder (kg/m^3)			Sand (kg/m^3)	Water (kg/m^3)	HRWR (lit/m^3)
Cement	GGBFS	MgO			
381.6	636	254.4	462	318	5–11

Table 2
Mixes considered in the present study.

Mix ID	PP fibre (vol %)	PE fibre (vol%)	Basalt fibre (vol %)
PP0PE0BF0	0	0	0
PP0PE2BF0	0	2	0
PP0.5PE2BF0	0.5	2	0
PP0PE1.25BF0.75	0	1.25	0.75
PP0PE1.25(9)BF0.75	0	1.25 (9 mm length)	0.75
PP0PE1.25(18) BF0.75	0	1.25 (18 mm length)	0.75
PP0.3PE1.25BF0.75	0.3	1.25	0.75
PP0.5PE1.25BF0.75	0.5	1.25	0.75

Note: Matrix constituents were kept fixed as shown in Table 1. PE fibre length is 12 mm unless otherwise specified.

Table 3
Properties of fibres used in the present study.

Fibre type	Length (mm)	Diameter (μm)	Tensile strength (MPa)	Elastic modulus (GPa)	Density (kg/m^3)
PE	9/12/18	24	3000	116	970
PP	12	23	585	5.1	910
Basalt	12	13	3300–4840	91–110	2650

scale fire studies on PE-ECC. Most research to date has focused on material-scale tests or applications as a protective coating [13–15]. This is primarily due to the complexity and high cost of large-scale furnace fire tests, which require specialized facilities. Additionally, material-scale tests on PE-ECC under elevated temperatures lack standardization, with variations in heating rates (1–10 °C/min) and specimen sizes (e.g. 50 mm cubes versus 75–100 mm diameter cylinders), complicating the understanding of its fire behaviour [2,16]. While recent advances have demonstrated the potential of ECC in structural applications such as beam-column joints, retrofitting, tunnel linings, and protective cladding [5,17,18], the use of PE-ECC and ECC in general in full-scale structures is still emerging. This highlights the need for a large-scale standardized and practical fire test to accurately assess its fire resistance and ensure broader applicability in construction.

This paper addresses these issues and systematically investigates the spalling resistance of PE-ECC developed with high-volume ground granulated blast furnace slag (GGBFS) as the primary supplementary cementitious material along with MgO, at both material and structural scale. The paper also details the development of a practical and standardized test setup for evaluating spalling resistance of panel specimens. A new one-directional (1-D) blow torch test method is introduced for this purpose and validated against three-directional (3-D) furnace fire test. The study further examines the effects of panel surface area, thickness, fibre combinations (including hybrid combinations with basalt or PP fibres), and different PE fibre lengths (9, 12, and 18 mm) on residual mechanical performance and spalling resistance. The insights into effective fibre combinations and spalling resistance mechanisms aim to enhance the practical application of PE-ECC in construction.

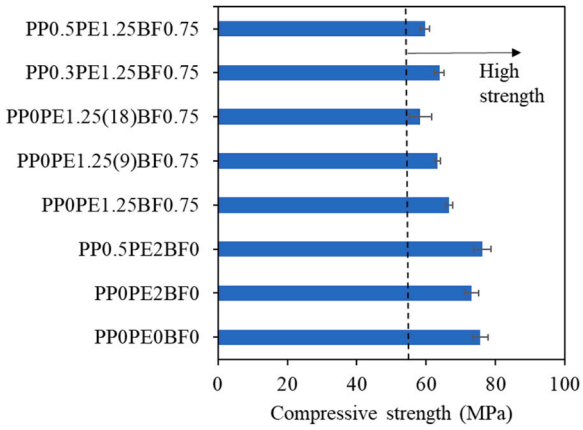

Fig. 2. Compressive strength of the considered mixes at room temperature.

Fig. 1. Mixing procedures adopted in present study.

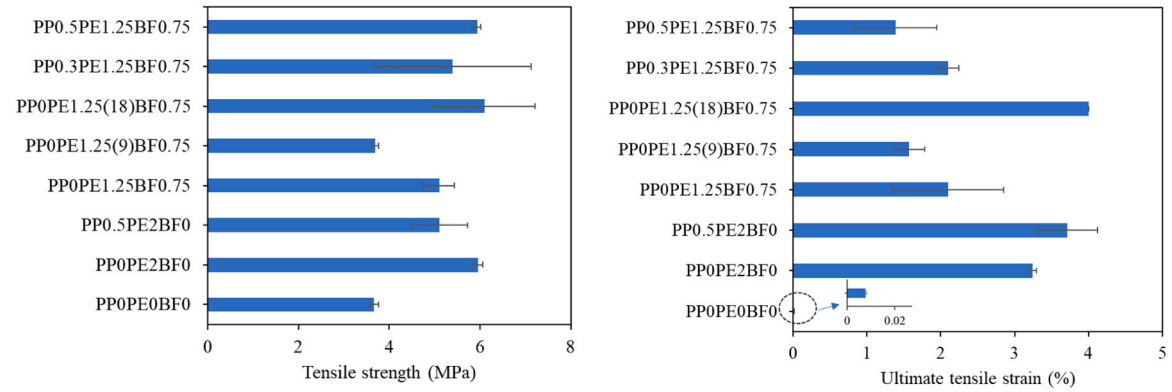

(a) Tensile strength (b) Ultimate tensile strain

Fig. 3. Tensile performance of the considered mixes at room temperature.

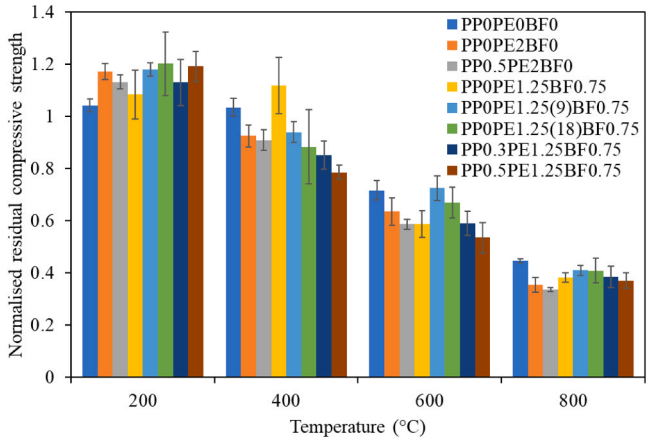

Fig. 4. Residual compressive strength of the mixes considered in the present study.

2. Material design and preparation

The primary binder materials used in this study were general-purpose (GP) cement, high-volume GGBFS as the main supplementary cementitious material, and MgO, which served as an expansive agent. GP cement and GGBFS complied with Australian Standards AS 3972 and AS 3582.2 respectively and were sourced as packaged products from a local supplier. MgO was obtained from QMAG, Queensland, with its properties detailed in the authors' previous work [19]. The ternary blend was also optimized for elevated temperature performance in this earlier study [19], and the same binder proportions (Cement:GGBFS: MgO = 30:50:20) were maintained for all mixes. 500 μm passing oven dried sand (specific gravity 2.64) was used as aggregate at a sand-to-binder ratio of 0.25. A carboxylated polymer-based high-range water reducer (HRWR), ADVA 650 (specific gravity 1.06), was also used to achieve consistent flow. The matrix constituents are further specified in Table 1.

Based on the outlined matrix constituents, eight different mixes with varying fibre contents were developed, as detailed in Table 2. The study focused on three types of fibres: PE fibre, PP fibre, and basalt fibre (BF), with their properties listed in Table 3. PP and basalt fibres were kept at a constant length of 12 mm, while PE fibres were used in three lengths of 9 mm, 12 mm, and 18 mm to study the effect of fibre length. The particular dosages for each fibre type were selected based on a comprehensive review of the literature and preliminary trials, which aimed to balance mechanical performance, spalling resistance and flowability. The control mix (PP0PE0BF0) contained no fibres. The mix PP0PE2BF0 included 2 % PE fibre by volume, which is considered the standard dosage in an ECC mix. Considering previous reports of poor spalling resistance in PE-fibre reinforced specimens and the superior fire performance of PP fibres [7], an additional 0.5 % PP fibre was introduced in mix PP0.5PE2BF0 to enhance fire resistance. Studies have also indicated that hybrid combinations of low and high melting point fibres improve elevated-temperature performance [20–22]. To explore this, mix PP0PE1.25BF0.75 was designed with 1.25 % PE fibre (melting point ~159°C) and 0.75 % basalt fibre (melting point >1000°C). This dosage was found to be optimal for room temperature performance in a previous study by the authors on another magnesium-based cement matrix [23]. Additionally, 12 mm length PE fibres in hybrid ECC mix were replaced with 9 mm and 18 mm length PE fibres to assess the effect of fibre length. To further enhance fire resistance, two additional hybrid mixes, PP0.3PE1.25BF0.75 and PP0.5PE1.25BF0.75, incorporated 0.3 % and 0.5 % PP fibres, respectively (melting point ~174°C). Since PP dosages above 0.1 % significantly improve spalling resistance [24–27], 0.3 % and 0.5 % were chosen as conservative estimates. Thus, these eight mixes were designed to assess not only the influence of PE fibre dosage but also the effects of hybrid basalt and PP fibres and the length of PE fibres in hybrid ECC, providing a comprehensive evaluation. Mix IDs follow the format PP*x*PE*y*BF*z*, where *x*, *y*, and *z* denote fibre volumes (%). PE fibre length defaults to 12 mm unless otherwise specified. For example, PP0PE1.25BF0.75 includes 0 % PP, 1.25 % PE (12 mm), and 0.75 % BF, whereas PP0PE1.25(18)BF0.75 denotes mix with 0 % PP fibre, 1.25 % PE fibre (18 mm), and 0.75 % basalt fibre.

A 40-litre planetary mixer was used for preparing the mixes, with the procedure illustrated in Fig. 1. The dosage of HRWR was adjusted within the supplier-recommended range for each mix to achieve consistent flow. For the base mix (PP0PE0BF0), the flow reached approximately 210 mm (spread diameter measured using the flow table test). However, with the addition of fibres, the flow decreased to about 160 ± 10 mm; mixes containing PP and PE fibres generally retained flow values toward the higher end of this range, whereas addition of basalt fibres slightly reduced flowability. Once the desired flow was reached, the mix was poured into the moulds designed for compression, tension, and spalling tests. 50 mm cube specimens were casted for compressive strength and residual compressive strength tests. Dog bone-shaped moulds, measuring 340 mm (length) × 50 mm (width) × 13 mm (thickness), were used to assess tensile stress-strain behaviour at both room and elevated temperatures. For spalling tests, panel moulds of sizes 300 × 300 × 50 mm, 200 × 200 × 50 mm, 100 × 100 × 50 mm and 300 × 300 × 20 mm were utilized. All specimens were demolded 24 hours after casting and then stored in a temperature-controlled water

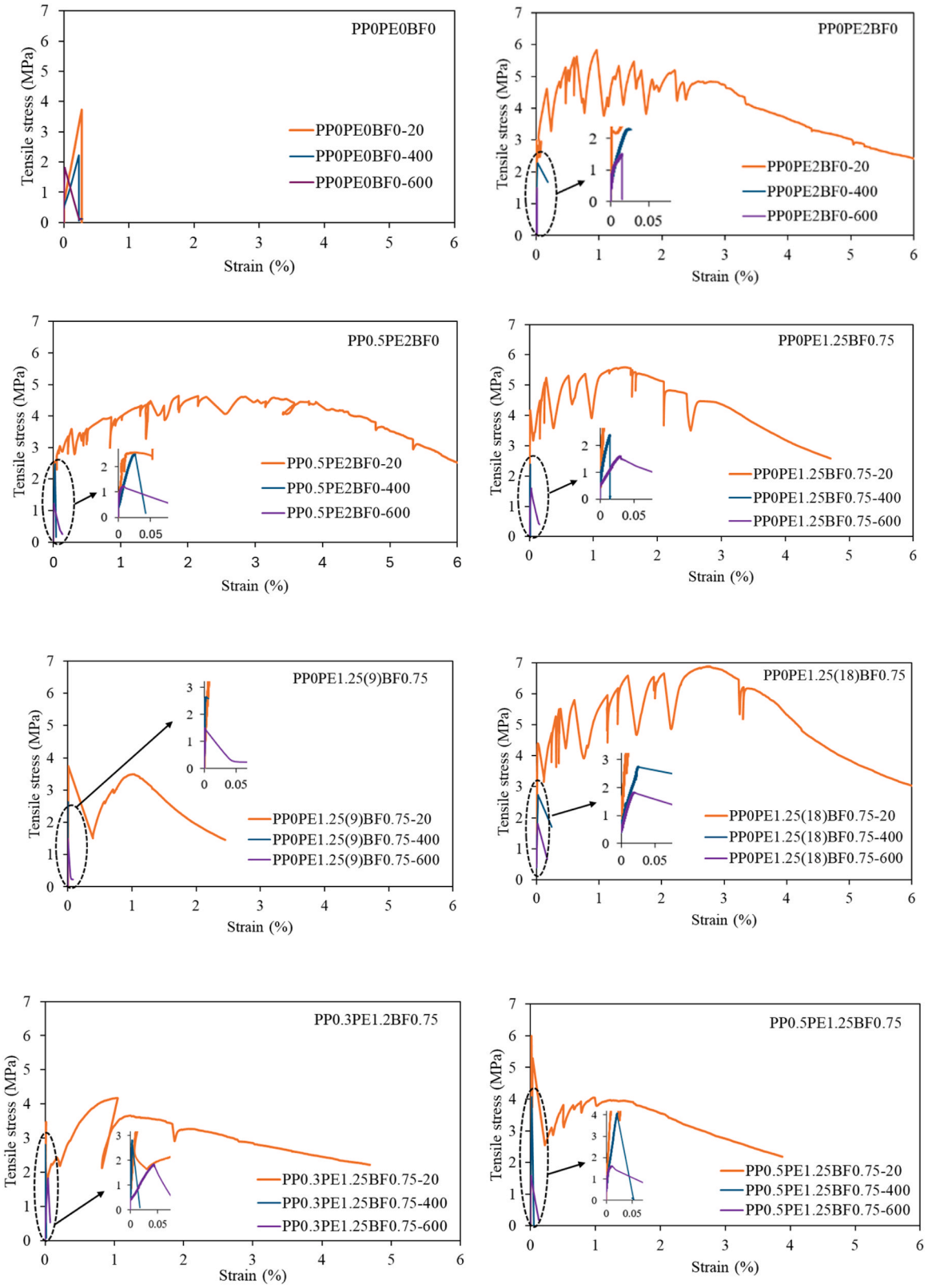

Fig. 5. Typical tensile stress-strain behaviour of considered mixes at room and elevated temperatures.

tank at 20 ± 2°C for 28 days. After the curing period, the specimens were taken out of the water tank and kept in an environmental chamber at 25 ± 2°C and 65 ± 5 % relative humidity until testing. The moisture content was measured prior to the testing phase by heating the specimens at 105 ± 2°C for 24 hours and it was found to be in a range of 5.9–6.5 % for all mixes. This measurement was performed to ensure that any extensive spalling observed could be correlated with the moisture content, if necessary.

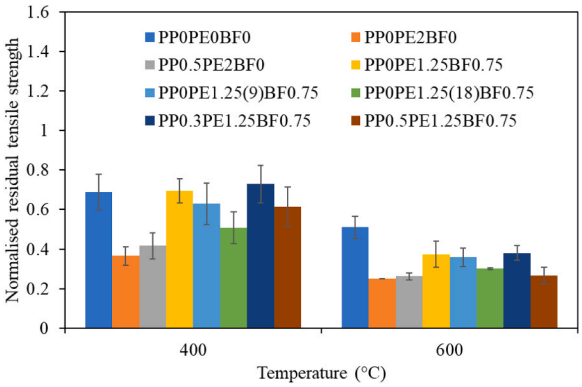

Fig. 6. Normalised residual tensile strength of ECC mixes.

3. Mechanical properties at room and elevated temperatures

The performance of the mix at both room temperature and elevated temperatures was first characterized to understand the general behaviour and correlate it further with spalling resistance, in order to recommend the most suitable fibre combination. For residual compressive strength, 50 mm cubic specimens were heated in a furnace to target temperatures of 200, 400, 600, and 800°C. Dog-bone specimens were heated to 400 and 600°C to analyse the residual tensile stress-strain behaviour. Heating rate was maintained at 2 °C/min and the temperature was monitored using two Type-K thermocouples, one attached to the specimen surface and the other positioned within the furnace, to confirm that the specimen temperature closely followed the furnace setpoint. After reaching each target temperature, a dwell period of 2 h was implemented to ensure an isothermal state, as suggested by Rawat et al. [16]. Following the dwell period, the specimens were allowed to cool naturally in ambient conditions by turning off the furnace and then kept in the same condition for 24 hours. Compression tests on the 50 mm cubes and uniaxial tension tests on dog-bone specimens (with a reduced width of 30 mm and a 60 mm gauge length) were then performed at a loading rate of 0.1 mm/min. The non-heated (room temperature) specimens were also tested at the same age to eliminate any effect of maturity. More details about the test setup can be found in Rawat et al. [28]. Three samples were tested for each set and temperature range to ensure representative results.

3.1. Mechanical properties at room temperature

3.1.1. Compressive strength

Fig. 2 shows the compressive strength of considered mixes at room temperature. The mortar mix (PP0PE0BF0) without fibres showed a compressive strength of 75 MPa. This might have been due to its better flow characteristics which have promoted better compaction and a more homogeneous matrix. In contrast, the incorporation of fibres introduces two competing effects on compressive strength. On one hand, the fibre bridging effect can enhance strength by limiting microcrack propagation; on the other hand, fibre agglomeration and the formation of voids may reduce matrix density, thereby lowering strength [29,30]. In the present study, the addition of 2 % PE fibre (PP0PE2BF0) did not significantly alter the compressive strength, likely because the fibres were well distributed and helped restrict crack propagation without significantly compromising the matrix density. Similarly, no further changes were observed when the same mix was further reinforced with an additional 0.5 % PE fibre.

However, replacing 0.75 % PE fibre with an equal volume of basalt fibres of the same length resulted in a 12 % reduction in compressive strength, likely due to basalt fibre agglomeration and the resulting increase in matrix porosity (as explained later in Section 6.3). The effect was also similar when length of PE fibre was changed to 9 mm. However, increasing PE fibre length from 12 mm to 18 mm at a constant fibre volume further reduced the strength by 8 %. Additionally, reinforcing mix PP0PE1.25BF0.75 with 0.3–0.5 % PP fibres did not improve the compressive strength, which remained lower than that of the mortar mix without fibres or the mix containing only polymer fibres.

3.1.2. Tensile strength and ultimate tensile strain

Fig. 3 shows the effect of fibre type and dosage on the tensile strength and ultimate tensile strain of ECC. Ultimate tensile strain was determined by recording the strain at the post-peak point where the load dropped to 75 % of the maximum tensile stress, as recommended in

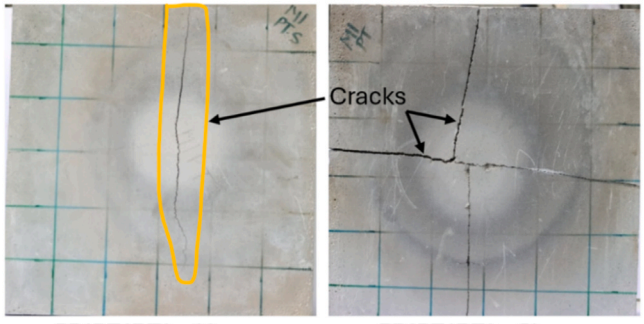

Fig. 8. Mix PP0PE0BF0 – 300 × 300 mm panel specimens after 1-D blow-torch test.

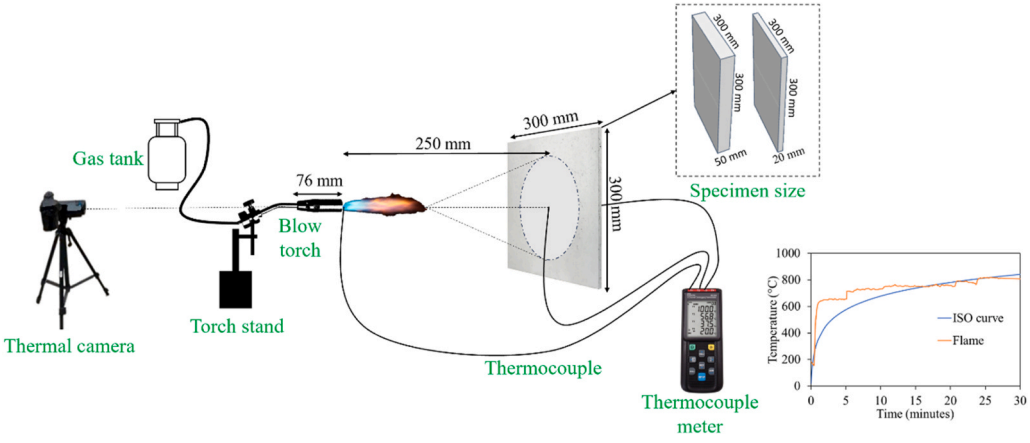

Fig. 7. Schematic diagram of the developed 1-D spalling test.

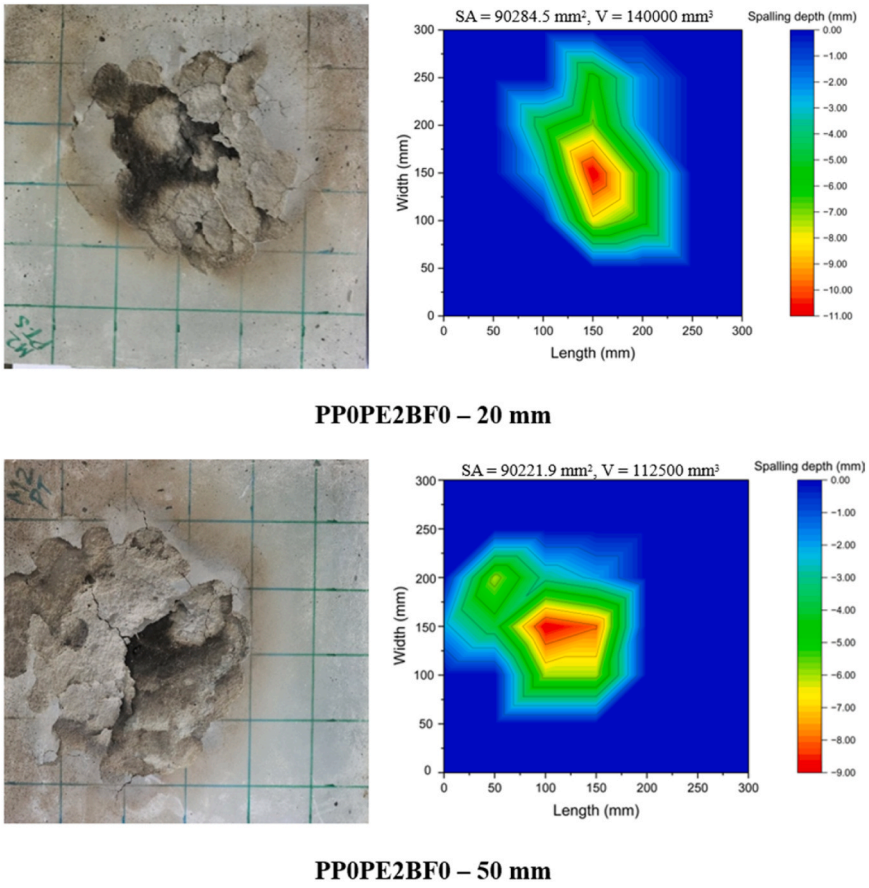

Fig. 9. Picture (left) and surface profile (right) of mix PP0PE2BF0 – 300 × 300 mm panel specimens after 1-D blowtorch test.

previous literature [31]. It can be seen that the mix PP0PE0BF0 without any fibre showed tensile strength of 3.6 MPa (Fig. 3a). However, the ultimate tensile strain was negligible due to the absence of fibres as expected (Fig. 3b). Adding 2 % PE fibre (PP0PE2BF0) resulted in an increase in both tensile strength and ultimate tensile strain, with tensile strength rising by 62 % to 6 MPa and ultimate tensile strain reaching approximately 3.3 %. Further addition of 0.5 % PP fibre (PP0.5PE2BF0) caused a slight decrease in tensile strength but led to an increase in ultimate tensile strain, which reached about 4 %. The improvements in both mixes were significant compared to the control mix and indicated their suitability for structural applications.

The effect of replacing PE fibres with an equal volume of basalt fibres was detrimental to both tensile strength and strain, consistent with the trend observed in compressive strength. Mix PP0PE1.25BF0.75, which replaced 0.75 % PE fibres with basalt fibres, showed approximately 36 % decrease in both tensile strength and ultimate tensile strain compared to mix PP0PE2BF0. The effect was more critical on changing the length of PE fibres. Using 9 mm fibres instead of 12 mm fibres maintained similar tensile strength but resulted in a notable decrease in ultimate tensile strain to less than 2 %. In contrast, using 18 mm fibres in hybrid ECC led to notable improvements in both tensile strength and ultimate tensile strain. Compared to the mix with 2 % PE fibre (PP0PE2BF0), tensile strength increased by 2 %, and strain capacity improved by 23 %, indicating that longer fibres can enhance tensile performance in hybrid ECC. These findings are particularly relevant for the development of cost-effective and environmentally friendly ECC, as basalt fibres not only have a more sustainable production process [32,33] but also exhibit lower embodied carbon emissions compared to PE fibres [34]. Any further addition of PP fibre to the mix with 12 mm hybrid fibres (1.25 %PE + 0.75 %BF) reduced tensile strain capacity, while tensile strength remained comparable to the mix with 2 % PE fibre.

3.2. Mechanical properties at elevated temperatures

3.2.1. Compressive strength

The residual compressive strength of all the mixes was measured at temperatures ranging from 200 to 800°C to assess how different fibre types and dosages affect strength retention. Notably, no spalling was observed in any of the specimens during the heating or the compression tests, which can be attributed to the optimized matrix composition [19] and the low heating-cooling rate employed. In terms of residual strength, it was observed that the compressive strength of all mixes significantly decreased with increasing temperature, especially beyond 600°C (Fig. 4). Especially, the compressive strength at 200°C was higher than at room temperature, with a more pronounced effect in fibre-reinforced specimens, showing an increase of 4–18 %. This improvement could be attributed to accelerated hydration in the high-SCM matrix at moderate temperatures, which results in pore refinement and enhanced strength [19]. However, as the temperature continued to rise, the compressive strength consistently decreased, with only about 34–44 % retention at 800°C.

If the residual strength between the mortar mix without fibres (PP0PE0BF0) and the fibre-based mixes including 2 %PE fibre (PP0PE2BF0), 2 %PE + 0.5 %PP (PP0.5PE2BF0) and 1.25 %PE + 0.75 %BF (PP0PE1.25BF0.75) is compared, it can be seen that all mixes showed an increase in compressive strength at 200°C. With further increase in temperature to 400°C, the strength decreased in some mixes, and the highest decrease was observed in case of PP0.5PE2BF0. The mix PP0PE2BF0 mix experienced a similar level of decrease, likely due to the complete melting of polymer fibres and subsequent vaporisation at higher temperatures. Interestingly, this effect was not

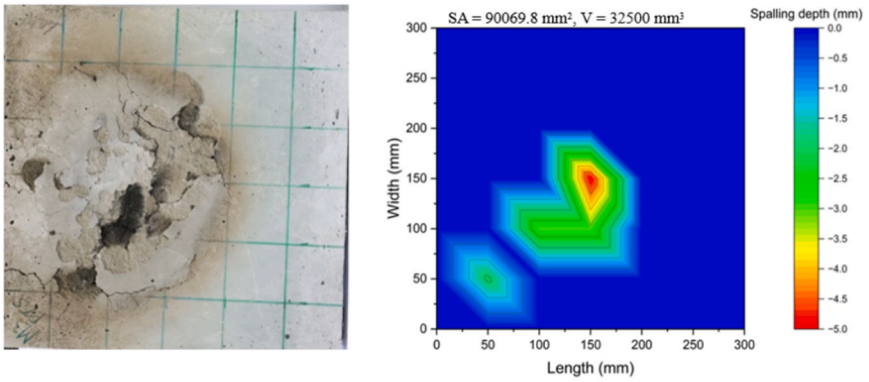

Fig. 10. Picture (left) and surface profile (right) of mix PP0.5PE2BF0 – 300 × 300 mm panel specimens after 1-D blowtorch test.

observed in the control mix (PP0PE0BF0), suggesting that GGBFS continued contributing to strength increase due to accelerated hydration. The effect was more pronounced in mixes with basalt fibres, likely due to improved fibre-matrix bonding. However, as the temperature exceeded 400°C, matrix deterioration became more significant, reducing the impact of the fibre-matrix bond and leading to a pronounced drop in strength, particularly in the fibre-reinforced mixes.

If the hybrid mixes PP0PE1.25BF0.75, PP0.3PE1.25BF0.75 and PP0.5PE1.25BF0.75 are compared, the effect of fibre melting could be clearly observed on residual strength. Beyond 200°C, the mix PP0PE1.25BF0.75 with least amount of polymer fibres showed lower reduction in comparison to the other mixes containing PP fibres. This difference can be attributed to the void formation or reduction in density caused by the melting of the PP fibres. Higher decrease was observed in mix PP0.5PE1.25BF0.75 with more PP fibres (0.5 %) in comparison to mix PP0.3PE1.25BF0.75 with lesser volume of PP fibres (0.3 %). As the temperature increased further, matrix degradation became the dominant factor, leading to a consistent reduction in strength across all mixes.

3.2.2. *Uniaxial tensile stress-strain behaviour*

The residual tensile stress-strain behaviour of all mixes was assessed at 400 and 600°C. These temperatures were selected based on the melting and vaporisation points of PE fibres to determine how PE fibres influence tensile stress-strain performance after exposure to high temperatures, and whether basalt fibres continue to offer benefits after PE fibres have vaporised. Fig. 5 shows the tensile stress-strain behaviour of the adopted mixes at room temperature and after exposure to 400°C and 600°C. The tensile strain hardening behaviour was clearly evident in all mixes except the base mix PP0PE0BF0. At elevated temperatures, this behaviour was completely lost and not only the tensile stress was found to decrease significantly, tensile strain also almost dropped to zero. This observed behaviour presents two inferences: first, the strain hardening behaviour is completely lost after the melting of PE fibre along with the reduced stress; second, the presence of basalt fibres did not have any appreciable effect even in providing necessary strain softening.

The effect of fibre dosage and different fibre types on residual tensile strength can further be observed from Fig. 6. The control mix PP0PE0BF0 without any fibre underwent 31 % reduction in tensile strength at 400°C which further reached 49 % at 600°C. The decrease was more severe in the mixes containing polymer fibres. Both PP0PE2BF0 and PP0.5PE2BF0 mixes suffered around 74 % reduction in the tensile strength at 600°C. The hybrid fibre mixes with lower content of polymer fibres and 0.75 % basalt fibres also underwent significant reduction at elevated temperatures, however, the performance was still better than the mixes with only polymer fibres. Mix PP0PE1.25BF0.75 suffered 63 % reduction in tensile strength at 600°C which was significantly better than the mixes with only polymer fibres.

A further comparison could be made for the mixes with different length of PE fibres. It can be observed that the longer PE fibres underwent slightly higher decrease in the tensile strength. Mix PP0PE1.25BF0.75 and mix PP0PE1.25(9)BF0.75 suffered around 63 % and 64 % decrease respectively at 600°C, whereas the reduction in the strength was 70 % for mix PP0PE1.25(18)BF0.75. Overall, the results highlight that the effect of elevated temperatures on tensile strength is primarily influenced by the dosage of polymer fibres and, to a lesser extent, their length. Higher polymer fibre dosage mixes showed greater strength reductions, likely due to increased voids from melted fibres. On the other hand, basalt fibres did not significantly improve the tensile strength, and there was no notable improvement in strain hardening or softening directly attributable to their inclusion.

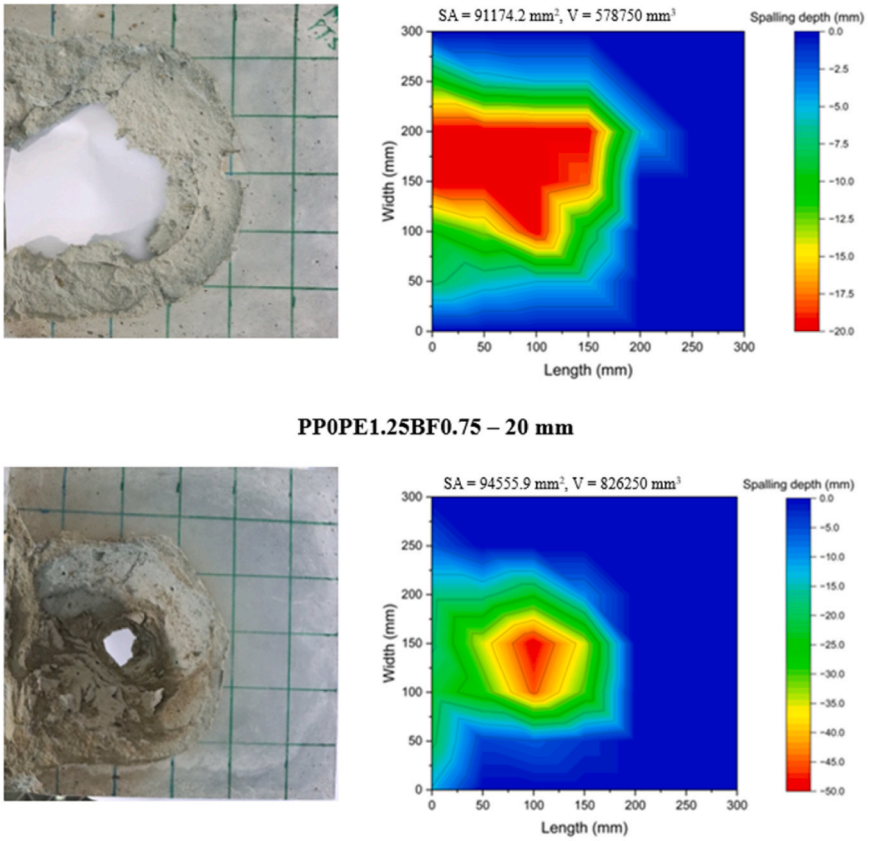

Fig. 11. Picture (left) and surface profile (right) of mix PP0PE1.25BF0.75 – 300 × 300 mm panel specimens after 1-D blowtorch test.

4. Spalling resistance testing via novel 1-D blow torch method

4.1. Development of cost-effective 1-D blow torch method

The 1-D blow torch method is usually conducted to simulate the effects of fire using a high temperature propane torch. Several studies have adopted similar testing methods to analyse the extent of spalling [4,35,36], however, these methods often lack consistency regarding the intensity of heating. To address this, repeated trials were conducted to match the ISO curve heating intensity so that the repeatability can be ensured in different tests. In this refined procedure, propane torch of nozzle diameter 33 mm and nozzle length 76 mm was selected for exposure on the ECC specimens with 300 mm × 300 mm surface area (20- and 50-mm thickness) to ensure adequate coverage. A larger area than this could lead to inefficient use of materials, while a smaller area might not capture the full flame intensity. The gas nozzle was fixed to a stand on a solid platform, and the nozzle-to-specimen distance was set at 250 mm. Type-K thermocouples were attached to the ECC specimens at different location (front and back centre) to monitor temperatures throughout the test. An additional thermocouple was embedded at the geometric centre of 300 × 300 × 50 mm specimen of mix PP0.5PE1.25BF0.75 to further understand the temperature profile. Temperature monitoring was also done using FLIR T865 thermal camera. A schematic diagram of the test setup is shown in Fig. 7. The notation 'Mix ID – thickness' is used hereafter to represent panel specimens, enabling easy comparison. For example, PP0PE0BF0 – 50 mm refers to the mix PP0PE0BF0 panel specimen with 50 mm thickness.

The test begins by igniting the blow torch at its lowest setting, causing a rapid increase in temperature (as shown in the temperature-time curve in Fig. 7). Once the temperature stabilizes, the flame control valve was adjusted gradually (by 10°) at the 5th, 20th, and 23rd minutes to achieve the desired temperature profile, with the test continuing for a total of 30 minutes. It should be noted that the test was designed to focus on thermal-hygral and potentially thermo-chemical spalling and hence, no external load was applied so that the stress generated by thermal gradients and vapour pressure could be clearly reflected. Throughout the heating process, temperature data from the thermocouples was recorded, and the surface of the concrete was observed for signs of spalling, such as cracking, popping, or flaking, with the respective times noted.

After the heating period, the blow torch was removed, and the ECC specimen was allowed to cool naturally. Once cooled, the specimen was inspected for the extent of spalling and any other damage. The surface profile data was plotted using OriginPro 2024b, where the profile was generated with the x-axis representing length, the y-axis representing width or height, and the z-axis representing depth or thickness. Additionally, the profile was employed to calculate the surface area (SA) of the xyz surface and the volume (V) between the plane at z = 0 and the matrix surface through two-dimensional integration. The primary advantage of this newly developed 1-D blow torch test method, with its standardized parameters, is that it offers a quick, cost-effective, and repeatable approach to simulate fire exposure and determine the spalling sensitivity of ECC specimens.

4.2. 1-D spalling test and analysis

4.2.1. Mortar without fibres (Mix PP0PE0BF0)

Fig. 8 shows the images of the specimens after undergoing exposure to fire through 1-D blow torch test. It is evident that both the 20 mm and 50 mm panel specimens did not exhibit any spalling, even in the absence

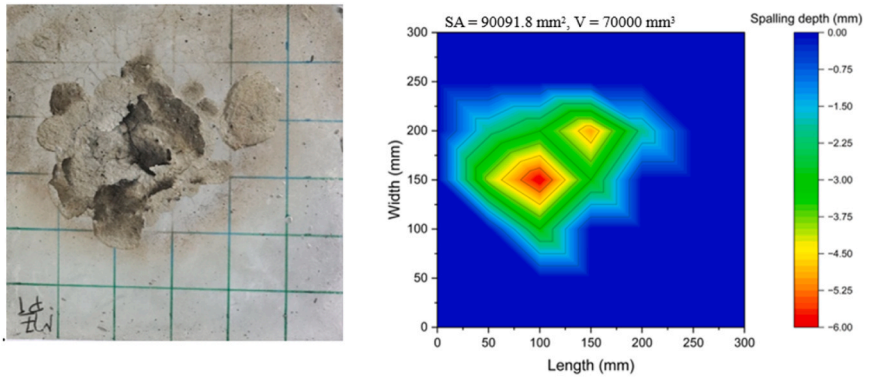

Fig. 12. Picture (left) and surface profile (right) of mix PP0.3PE1.25BF0.75 – 300 × 300 mm panel specimens after 1-D blowtorch test.

of fibres. This absence of spalling is likely due to the less-dense internal microstructure, which resulted from incomplete hydration caused by the very high SCM content (70 % replacement) [19]. Consequently, the formation of a dense matrix that would trap vapours did not occur, allowing vapour pressure to dissipate easily from the unexposed sides. However, specimens fractured right after the test, suggesting that mortar alone is insufficient to prevent disintegration, and the addition of fibres could be beneficial.

4.2.2. Mix with low melting point polymer fibres (Mix PP0PE2BF0 and PP0.5PE2BF0)

To understand the effect of 1-D fire exposure on ECC reinforced with low melting point fibres, 20- and 50-mm thick panel specimens were tested for mix PP0PE2BF0 and PP0.5PE2BF0. Unlike the mix without fibres, these specimens exhibited minor surface spalling, as shown in Fig. 9. The figure also presents surface profile detailing the extent of damage, including the front-facing damage area and the spalled depth (represented separately along the z-axis). As observed in the surface profile, the maximum spalling depth was 9 mm for 50 mm specimens and approximately 11 mm for 20 mm specimens. In both thicknesses, spalling began at the start of the test and continued for only the initial 3–4 minutes (when the temperature was likely below 500°C), after which spalling completely stopped even though the temperature continued to rise due to flame exposure. Unlike the specimens without any fibre, where incomplete hydration and a more porous structure facilitated easier vapour escape, the addition of uniformly distributed PE fibres likely resulted in a denser matrix through improved packing or reduced porosity. Though fibres started melting upon heating, they may not have initially formed a continuous network of escape channels for vapour release. This could have led to localized pressure accumulation, causing early-stage spalling. However, as the test progressed, a network of interconnected voids was likely formed due to fibre decomposition and fibre-matrix bond degradation, facilitating vapour dissipation and thereby preventing further spalling. The surface profile was further used to calculate the spalled volume and SA. The spalled volume was 140,000 mm^3 for the 20 mm specimens and 112,500 mm^3 for the 50 mm specimens, while the SA was 90,285 mm^2 and 90,222 mm^2 for the 20 mm and 50 mm thickness specimens, respectively.

Further reinforcing the specimens with 0.5 % PP fibre (PP0.5PE2BF0) resulted in a slight improvement in spalling resistance. As shown in Fig. 10, both 20 mm and 50 mm thick specimens experienced only minor surface spalling, with the maximum spalling depths of 5 mm and 10 mm, respectively. The improvement was more pronounced in the 20 mm specimens, where the spalled volume decreased by 76 % compared to the PP0PE2BF0 mix, likely due to better interconnected network of channels and smaller moisture migration paths due to lower thickness. However, the profile geometry of the 50 mm specimens showed no significant change, and the damage surface area was similar to the PP0PE2BF0 specimens. Spalling still occurred for a similar duration, starting at the beginning of the test and continuing for only 3 minutes. Additionally, a popping sound was observed in the 50 mm specimens at 10 and 12 minutes, but this did not cause significant additional damage and only removed the already compromised outer layer. Overall, the presence of low melting point PE fibres in the standard 2 % dosage in ECC greatly reduces the likelihood of major spalling. Further addition of PP fibre may also slightly improve the spalling resistance depending on the size of the specimens.

4.2.3. Hybrid ECC with low and high melting point fibres

The spalling resistance of ECC reinforced with a combination of basalt and PE fibres was also examined to assess whether basalt fibres could serve as a cost-effective, environmentally friendly alternative. It

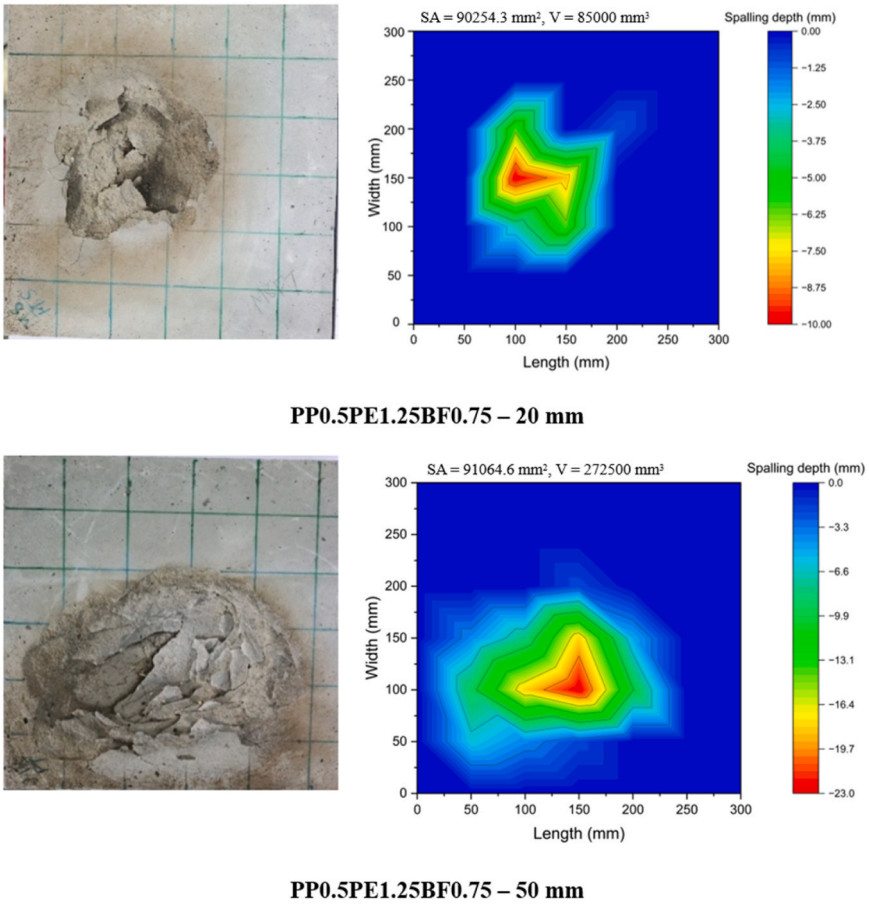

Fig. 13. Picture (left) and surface profile (right) of mix PP0.5PE1.25BF0.75 – 300 × 300 mm panel specimens after 1-D blowtorch test.

was found that ECC panels with 1.25 % PE and 0.75 % basalt fibre (PP0PE1.25BF0.75) spalled through the full thickness under 1-D exposure, irrespective of panel thickness (Fig. 11). This suggests that the selected fibre combination was not effective in preventing spalling, despite its superior performance under lower heating rates (Figs. 4 and 6). These findings further highlight the importance of 1-D spalling test in material development, as it is simple to implement and offers a reliable means of assessing spalling resistance. Such testing is crucial for accurately identifying ECC mixes that offer both high residual strength and enhanced resistance to spalling.

In terms of spalling extent, spalling began immediately in 50 mm specimens and continued explosively for 19 minutes until the flame had penetrated the entire thickness, at which point the test was stopped. For the 20 mm specimens, spalling also started at the beginning of the test and the full thickness was spalled within 12 minutes. The surface profile volume for the 20 mm specimens showed a 313 % increase compared to the PP0PE2BF0 mix, whereas the 50 mm specimens demonstrated a 634 % increase. This severe spalling can be attributed to two primary factors. First, unlike PE or PP fibres, which melt at relatively low temperatures and have lower bonding with the matrix, basalt fibres remain intact due to their high melting point and exhibit strong bonding with the matrix. While this might contribute to better residual strength, it prevents the formation of a well-distributed network of voids needed for effective vapour pressure relief, causing pressure buildup and explosive spalling. Second, basalt fibres tend to agglomerate, which further disrupts uniform channel formation and exacerbates internal stress buildup. These results highlight the inadequacy of this commonly adopted hybrid fibre dosage in providing sufficient spalling resistance under 1-D fire exposure.

Small amounts of PP fibres were further added to improve spalling resistance as this addition doesn't significantly increase the cost or compromise room temperature mechanical properties. As shown in Fig. 12, the addition of just 0.3 % PP fibre (PP0.3PE1.25BF0.75) led to a substantial improvement in spalling resistance. Both 50 mm and 20 mm thick panel specimens exhibited only minor surface spalling, with a maximum spalling depth of 5–6 mm. In the 50 mm thick panels, spalling was observed for the first 4 minutes, while in the 20 mm panels, it ceased after 6 minutes. The surface profile volume also decreased by 87 % for the 20 mm thick panels and by 96 % for the 50 mm thick panels compared to the PP0PE1.25BF0.75 mix, and the performance was also found better than mix PP0PE2BF0.

Increasing the dosage of PP fibres to 0.5 % also improved spalling resistance compared to the PP0PE1.25BF0.75 mix. However, the performance was slightly inferior to the PP0.3PE1.25BF0.75 mix. This effect was more pronounced in the 50 mm thick panel specimens, which experienced a maximum thickness loss of 26 mm due to spalling (Fig. 13). Spalling began at the start of the test and continued for 16 minutes before stopping completely. Notably, spalling only continued until the embedded thermocouple was exposed and stopped afterward, suggesting that the discontinuity caused by the thermocouple embedment (due to the difference in material properties) might have contributed to this effect rather than the fibre itself. For the 20 mm thick panel specimens, the effect of fibre dosage was more evident. Spalling began 2 minutes into the test and only lasted for 8 minutes, resulting in a 10 mm thickness loss. The surface profile volume decreased by 85 % for the 20 mm thick panels and by 67 % for the 50 mm thick panels compared to the PP0PE1.25BF0.75 mix. However, this performance was not as effective as that achieved with the PP0.3PE1.25BF0.75 mix. Overall, the results indicate that adding PP fibre may significantly improve the spalling resistance and with the appropriate choice of fibre

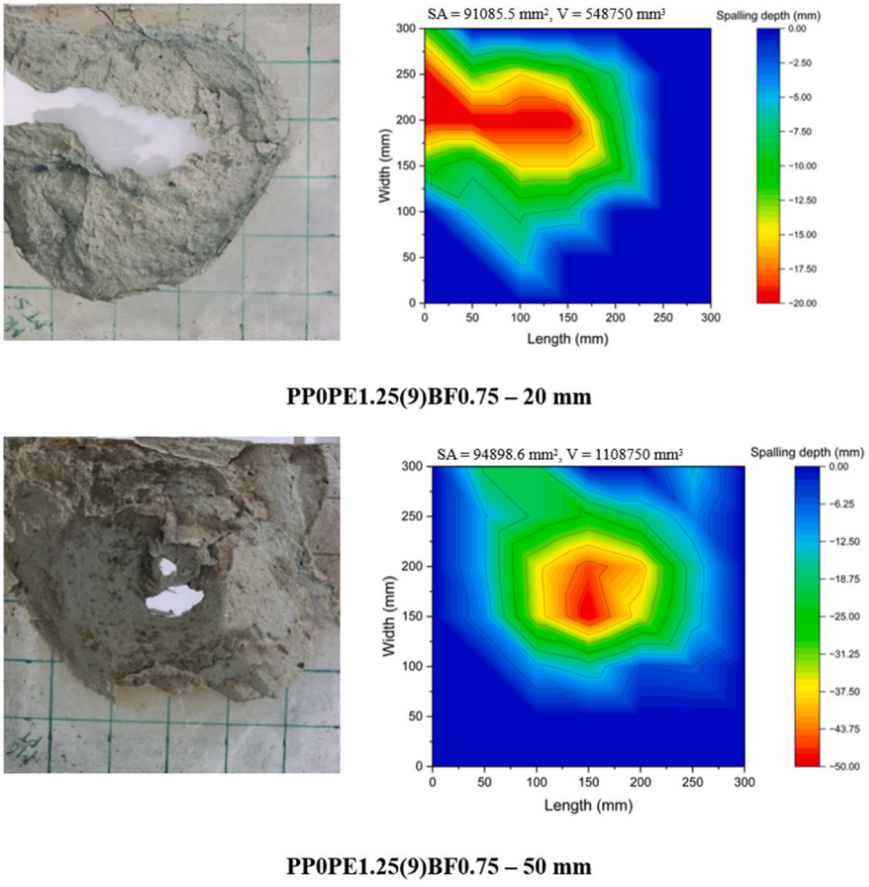

Fig. 14. Picture (left) and surface profile (right) of mix PP0PE1.25(9)BF0.75 – 300 × 300 mm panel specimens after 1-D blowtorch test.

type and dosage, spalling resistance can be substantially enhanced without compromising room temperature and residual performance.

4.2.4. Hybrid ECC with different lengths of PE fibre

Since full thickness explosive spalling was observed in the mix PP0PE1.25BF0.75 (with 12 mm PE fibre length), further analysis was conducted with different fibre lengths to determine if spalling resistance could be improved by changing the fibre length. When replacing the 12 mm fibres with 9 mm fibres in mix PP0PE1.25(9)BF0.75, the specimens still experienced full thickness spalling in both 20 mm and 50 mm panel specimens (Fig. 14). Additionally, the spalled area was larger compared to specimens with 12 mm PE fibres. In the 50 mm specimens, full thickness spalling occurred at the 27th minute, while the 20 mm specimens exploded suddenly at the 13th minute. The profile volume of the 20 mm thick specimens was comparable to the mix PP0PE1.25BF0.75, but this volume significantly increased (by 34 %) for the 50 mm thick specimens. This indicates that 9 mm fibres were ineffective and confirms that shorter fibres may not contribute effectively to the formation of interconnected network of channels.

For 18 mm PE fibre specimens (PP0PE1.25(18)BF0.75), spalling resistance was found to be greatly improved. 50 mm specimens did not experience complete spalling, although spalling continued throughout the 30-minute test, reaching a maximum spalled thickness of 32 mm (Fig. 15). The effect was less severe for the 20 mm specimens, where spalling occurred only during the first 5 minutes of the test, causing minor damage with a thickness of 6 mm before stopping. The spalled volume also decreased by 93 % for the 20 mm thick specimens compared to the PP0PE1.25BF0.75 mix, while the reduction was 27 % for the 50 mm specimens. These results further confirm that decreasing the fibre length (at constant diameter) does not positively affect spalling resistance, whereas increasing the fibre length may improve spalling resistance, possibly due to a better network of channels.

5. Spalling resistance of ECC: 3-D exposure test and analysis

5.1. 3-D fire test

The 3-D heating test or the furnace heating test involved placing ECC specimens in a furnace where they were subjected to elevated temperature to mimic ISO 834 standard fire curve as shown in Fig. 16. The heating rate and duration were carefully controlled to match the standard rate, and temperature data was continuously recorded using Type-K thermocouples placed at various locations in the furnace and on the specimen surfaces. After reaching the target temperature of 800°C, the specimens were held at this temperature for a total test duration of 30 minutes. Subsequently, the specimens were cooled naturally and analysed for the extent of spalling and other damages after 24 hours. The surface profile was also drawn for any spalled specimens using the previously described method. ECC specimens with varying thickness (at constant surface area) 300 × 300 × 50 mm and 300 × 300 × 20 mm as well as specimens with varying cross section area (at constant thickness) 200 × 200 × 50 mm and 100 × 100 × 50 mm were also considered to analyse the individual effect of these parameters. Additionally, 50 × 50 × 50 mm cubic specimens were exposed to this higher rate of fire heating to further compare the results with those from specimens exposed to lower heating rate. Overall, the 3-D exposure test provides uniform heating, better replicating real fire scenarios, and accommodates larger specimens, but is more expensive and time-consuming, requiring specialized equipment and facilities.

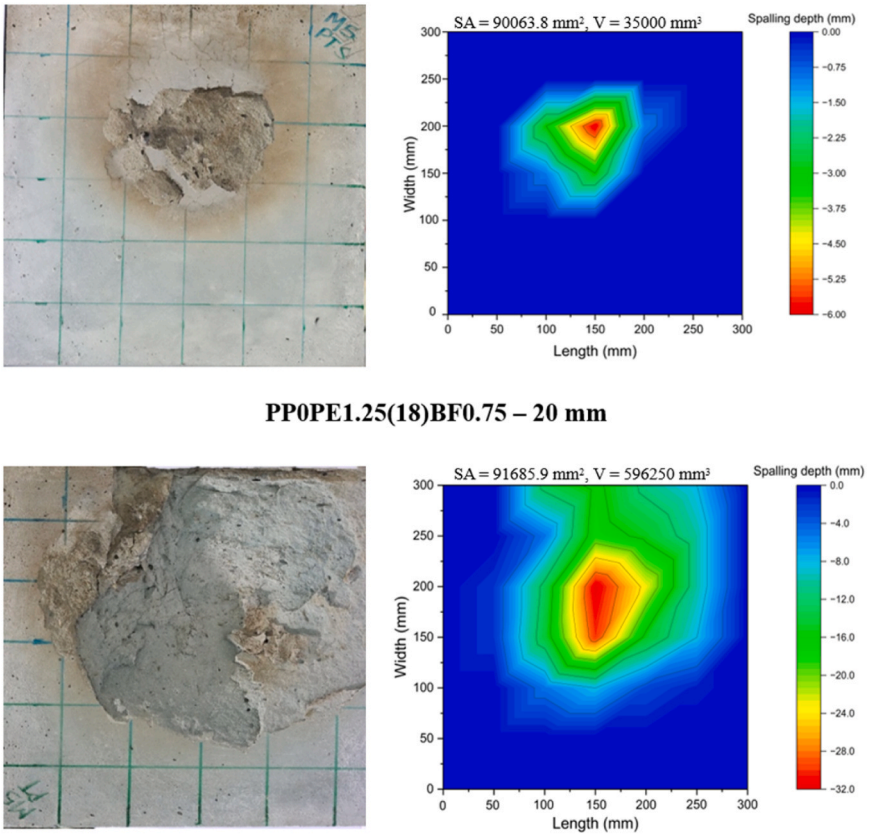

Fig. 15. Picture (left) and surface profile (right) of mix PP0PE1.25(18)BF0.75 – 300 × 300 mm panel specimens after 1-D blowtorch test.

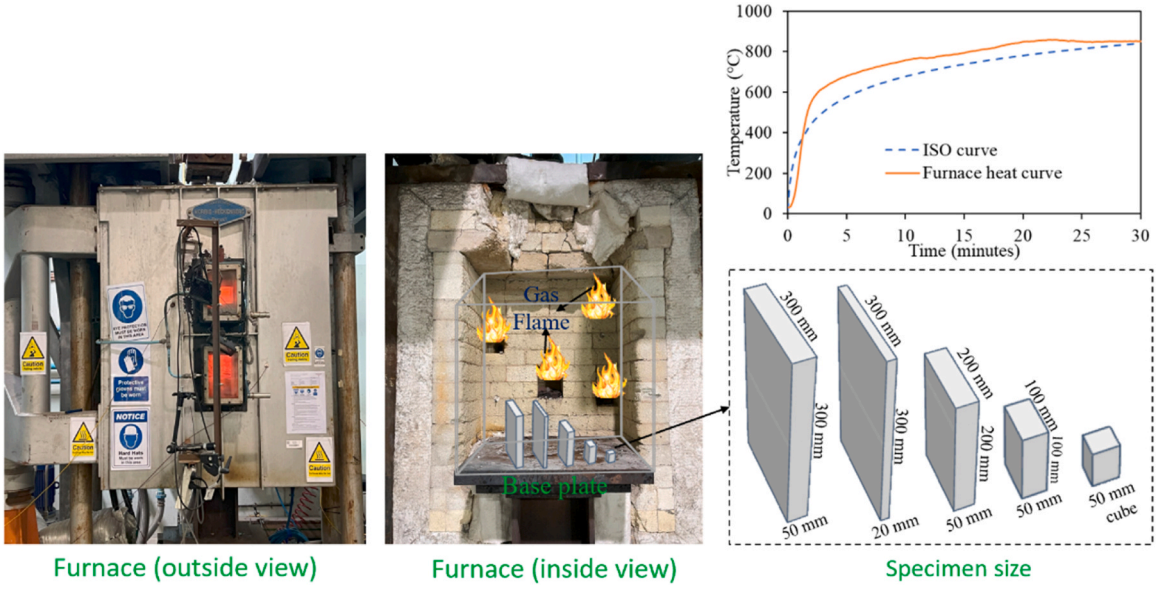

Fig. 16. 3-D fire test setup for spalling.

5.2. 3-D spalling test results and analysis

5.2.1. Mortar without fibres (Mix PP0PE0BF0)

Similar to the behaviour observed under 1-D exposure, the 50 mm panel specimen without any fibre (PP0PE0BF0) suffered extensive cracks and disintegrated after exposure (Fig. 17). Although the 20 mm thick specimens were not completely broken, they still showed major cracks on both sides and broke as soon as the panel was put down after testing. The observed disintegration is consistent with the 1-D test and may have been due to the inability of the porous matrix to effectively manage thermal stresses and vapour pressure, confirming that fibre reinforcement is critical for maintaining material integrity under fire

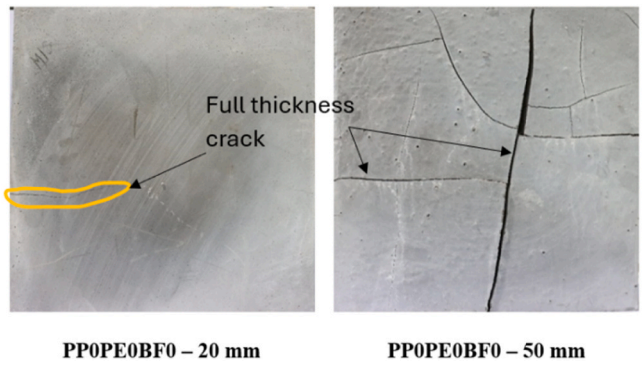

Fig. 17. Mix PP0PE0BF0 – 300 × 300 mm panel specimens after 3-D exposure test.

exposure.

5.2.2. Mix with low melting point polymer fibres (Mix PP0PE2BF0 and PP0.5PE2BF0)

Panel specimens with only low melting point polymer fibres (PP0PE2BF0 and PP0.5PE2BF0) did not experience major spalling. Only minor surface spalling and visible cracks were observed, as shown in Fig. 18. Both mixes (with 2 % PE fibres and hybrid 2 % PE + 0.5 % PP fibres) exhibited similar behaviour for specimens of the same thickness. In the 50 mm specimens, minor surface spalling occurred along with significant cracking. In contrast, the 20 mm specimens did not undergo any spalling but displayed one major crack extending from the centre to one end, along with some minor cracks. This difference might be due to the easier dissipation of pore pressure in the thinner specimens, while the thicker specimens experienced prolonged exposure to pore pressure buildup, resulting in more cracks. However, the network of channels due to fibres was still sufficient to release the pore pressure.

5.2.3. Hybrid ECC with Low and high melting point fibres

The effect of hybrid ECC with PE and basalt fibre under 3-D fire exposure was further analysed. In the 50 mm panel specimens for mix PP0PE1.25BF0.75, significant spalling occurred at one end (occurring within first 5 minutes of test), along with minor surface spalling and major cracks (Fig. 19). In contrast, the 20 mm specimens only showed major cracks. When these specimens were reinforced with 0.3 % and 0.5 % PP fibres, only major cracks were observed, with no visible spalling. The same effect was observed in the 20 mm specimens, which also did not suffer any apparent major cracks. Notably, the spalling behaviour observed under 3-D exposure was consistent with the trends obtained from the 1-D tests. However, it is worth noting that under 1-D fire exposure, the same hybrid mix (PP0PE1.25BF0.75) underwent full-

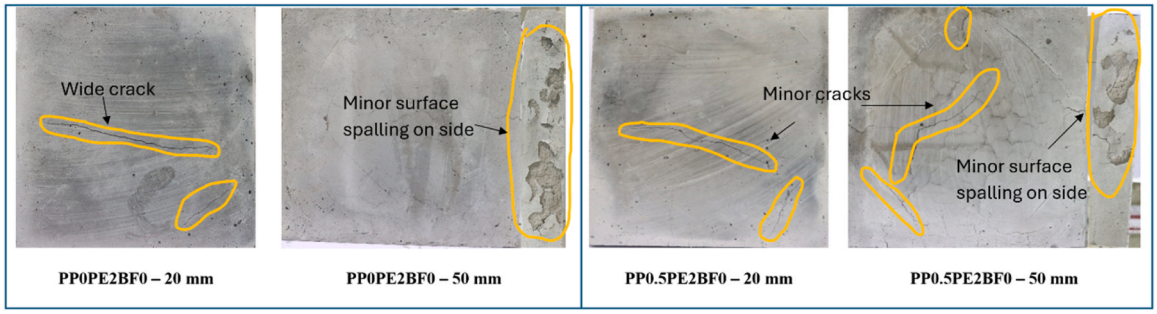

Fig. 18. Mix PP0PE2BF0 and PP0.5PE2BF0 – 300 × 300 mm panel specimens after 3-D exposure test.

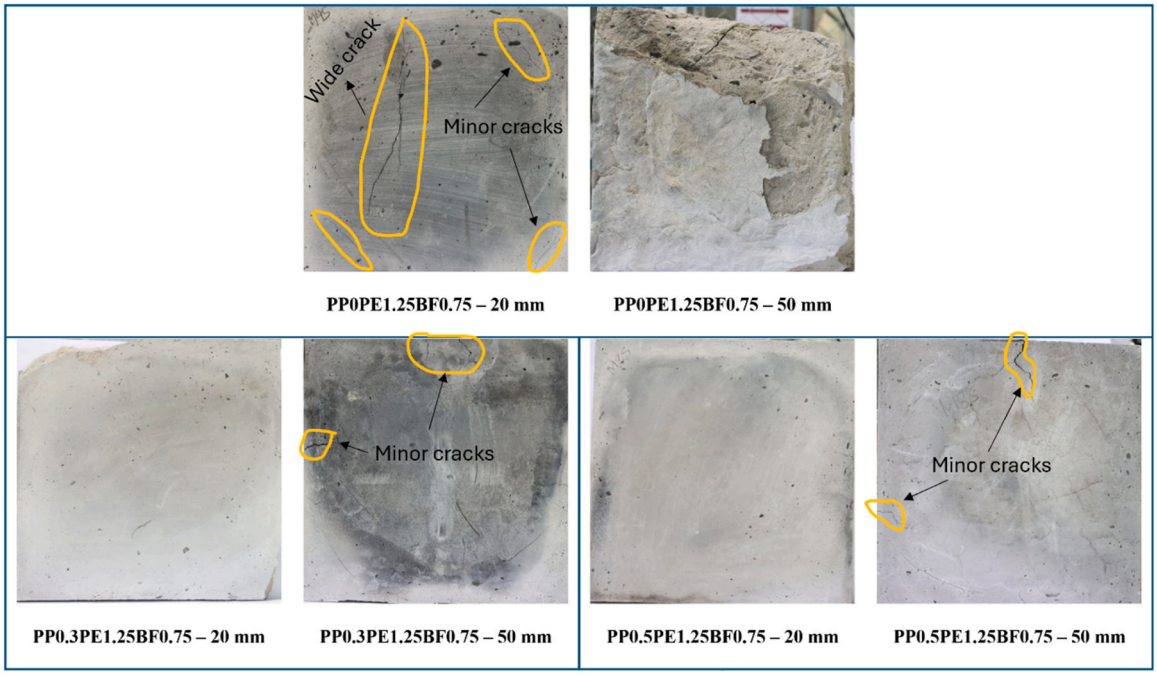

Fig. 19. Mix PP0PE1.25BF0.75, PP0.3PE1.25BF0.75 and PP0.5PE1.25BF0.75 – 300 × 300 mm panel specimens after 3-D exposure test.

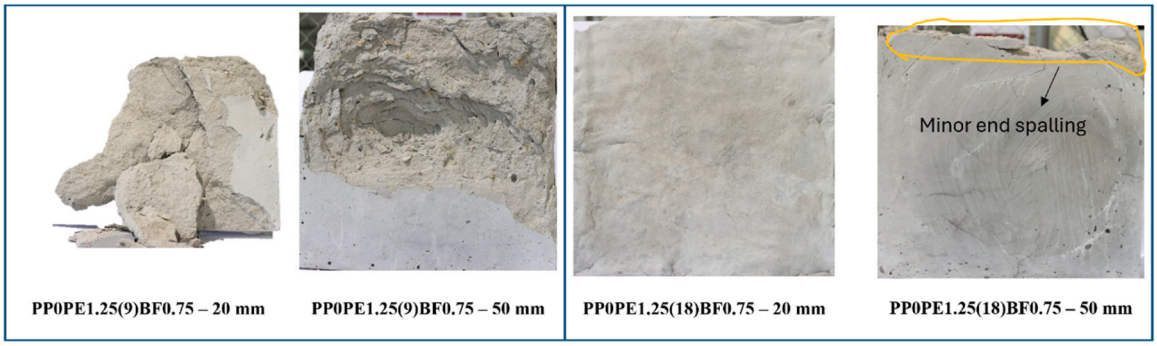

Fig. 20. Mix PP0PE1.25(9)BF0.75 and PP0PE1.25(18)BF0.75 – 300 × 300 mm panel specimens after 3-D exposure test.

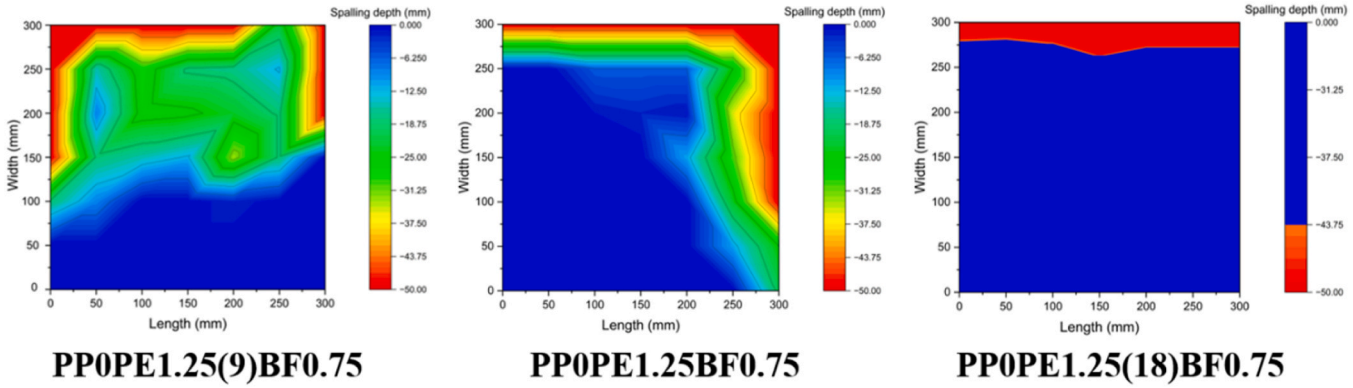

Fig. 21. Surface profile of 300 × 300 × 50 mm panel specimens of hybrid PE and basalt fibre mixes after 3-D exposure test.

thickness spalling. This discrepancy is likely due to the different exposure conditions: under 1-D exposure, heating is unidirectional, making spalling behaviour highly dependent on mixing conditions, fibre–matrix bonding, and the degree to which fibres decompose to form continuous vapour-release channels. In contrast, 3-D exposure heats the specimens from all sides, facilitating the formation of a more continuous network of channels for vapour escape and thus reducing the severity of spalling. Nevertheless, the occurrence of spalling in PP0PE1.25BF0.75 under 3-D conditions confirms that the 1-D test also provides an accurate prediction of spalling behaviour, further affirming its reliability as a testing method.

5.2.4. *Hybrid ECC with different lengths of PE fibre*

When 12 mm PE fibres were replaced with 9 mm fibres while maintaining the same total dosage (PP0PE1.25(9)BF0.75), spalling was observed in both 20 mm and 50 mm panel specimens as shown in Fig. 20. The spalling sound was heard for initial 3–5 minutes of the test and the resulting explosion was found to be very severe in both thicknesses, suggesting that the 1.25 % dosage was insufficient for the 9 mm fibres to create a connected network of channels necessary for pore dissipation. On the other hand, when PE fibre length was increased to 18 mm, only end spalling was noted, and the performance was better compared to the 12 mm fibre specimens. A further comparison can be made of the surface profile of 50 mm panel specimens for the mixes with different fibre lengths (Fig. 21). The profile clearly shows significantly more spalling in the 9 mm PE fibre specimens than in the 12 mm and 18 mm fibre specimens. These results also align with those from the 1-D exposure tests, suggesting that increasing fibre length at a fixed dosage may enhance spalling resistance.

5.3. *Spalling resistance of varying sized panels (3-D exposure test)*

The effect of specimen surface area on spalling resistance was analysed by comparing 100 × 100 × 50 mm and 200 × 200 × 50 mm panels under 3-D exposure. As shown in Fig. 22, specimens without fibres developed cracks similar to those of the larger surface area specimens; however, their integrity remained intact in both sizes. Comparing these with 300 mm specimens, it is evident that crack intensity decreased as the surface area decreased across all mixes. The 300 × 300 × 50 mm specimens experienced the highest intensity of cracks, followed by the 200 × 200 × 50 mm and 100 × 100 × 50 mm specimens.

Mix with 2 % PE fibre (PP0PE2BF0) exhibited varying effects for different sizes. Larger specimens of 300 mm and 200 mm experienced surface spalling, whereas the 100 mm specimens only had minor cracks. The same pattern was observed for the mix PP0.5PE2BF0, where 100 mm specimens showed no spalling or cracks, but surface spalling was visible in the 300 mm specimens. The effect was more pronounced for hybrid fibre-reinforced specimens. For 12 mm length PE fibre hybrid ECC specimens (PP0PE1.25BF0.75), spalling occurred in both 300 mm and 200 mm specimens, whereas 100 mm specimens showed no observable spalling. A similar effect was noted for specimens with 9 mm PE fibre (PP0PE1.25(9)BF0.75). The 18 mm length PE fibre (PP0PE1.25(18)BF0.75) specimens did not show any spalling in the 200 mm or 100 mm specimens but exhibited side spalling in the 300 mm specimens. The spalling in PP0PE1.25BF0.75 was also mitigated with the addition of PP fibres (PP0.3PE1.25BF0.75 and PP0.5PE1.25BF0.75).

Overall, these findings indicate that the exposed surface area critically affects spalling resistance and crack propagation. As the surface area decreased, the tendency for spalling significantly reduced, and the 100 × 100 × 50 mm specimens did not experience any spalling irrespective of the fibre dosage or type. Furthermore, crack intensity also decreased with a reduction in the exposed area of the specimen.

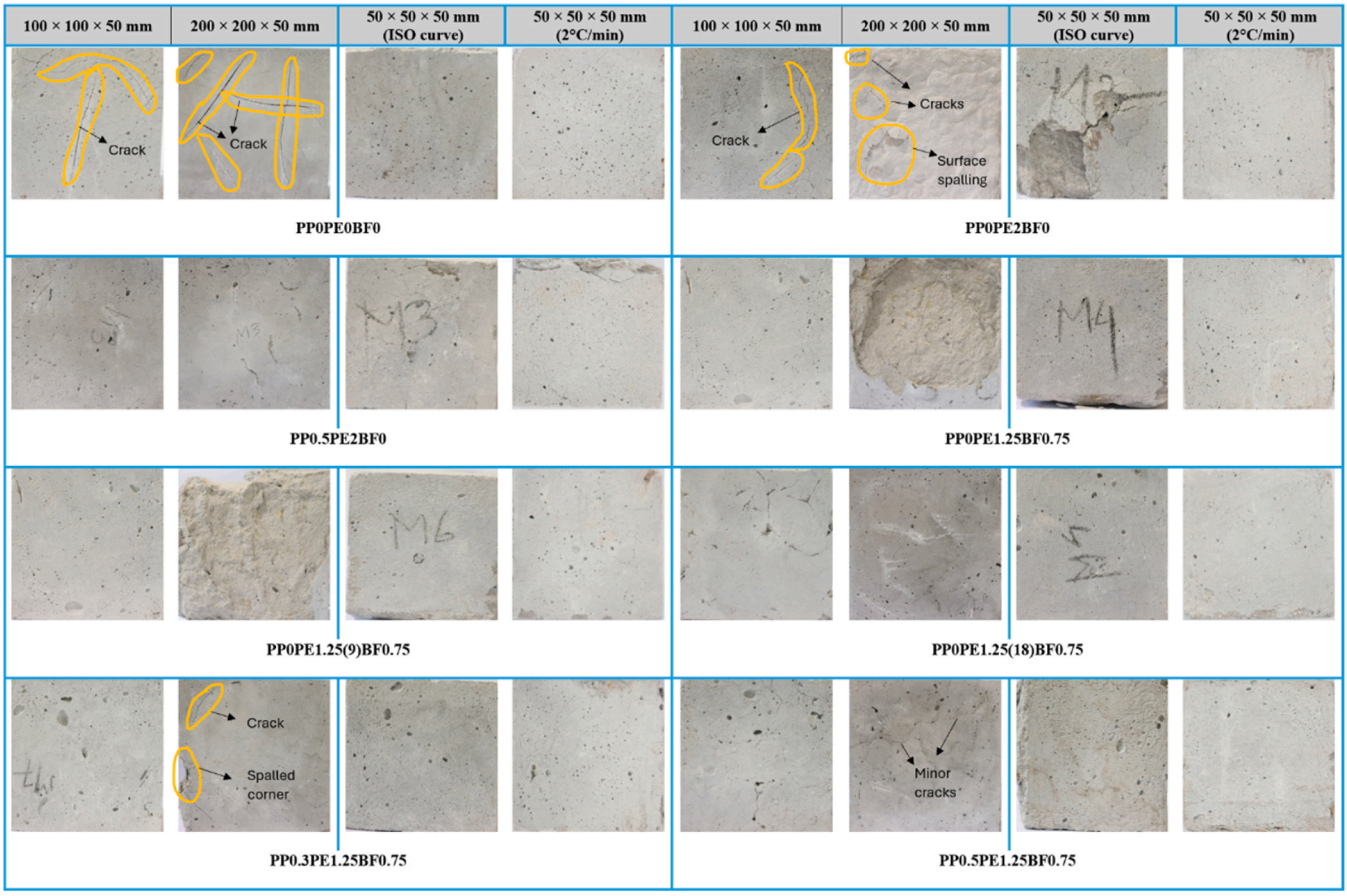

Fig. 22. Comparison of spalling in different sized specimens with 50 mm thickness (Note: The front surface shown depicts the full surface area of each specimen).

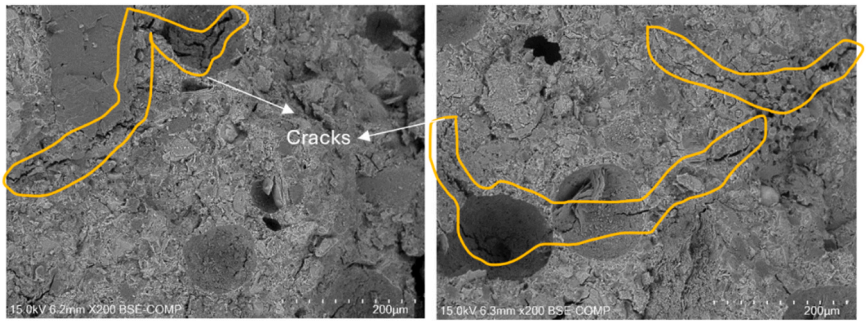

Fig. 23. Microstructure of PP0PE0BF0 mix after 1-D fire exposure.

5.4. Effect of heating profile (3-D exposure test)

The effect of heating rate was assessed by comparing the surface profiles of 50 mm cubes subjected to ISO curve heating and low-rate heating (2 °C/min) to 800°C. As can be seen from Fig. 22, 50 mm cubic specimens did not exhibit spalling at either heating rate, with the exception of the PP0PE2BF0 specimens, which showed minor surface spalling in only one of the three specimens tested. This suggests that the heating rate effect may not be as pronounced in smaller cubic specimens, which are commonly used in elevated temperature studies. Additionally, crack propagation could not be clearly compared in these small cubes. Therefore, for a more effective investigation of spalling resistance, larger specimens should be used.

6. Spalling mechanism in single or hybrid fibre reinforced PE-ECC

The experimental results demonstrate that the spalling behaviour of ECC is strongly influenced by fibre dosage, type, and distribution, as well as specimen size. For instance, incorporating 2 % PE fibres effectively prevented major spalling, whereas a hybrid mix with 1.25 % PE (12 mm) and 0.75 % basalt fibres failed to provide sufficient resistance despite exhibiting superior residual strength. Although moisture content is often cited as a key factor affecting spalling, all specimens in this study maintained a similar moisture range (5.9–6.5 %), indicating that differences in spalling behaviour may not be due to moisture variability. Moreover, the absence of spalling in mortar specimens indicates that the microstructure was less dense even before fire exposure and the crack formation under fire (as shown in Fig. 23) might have allowed pore pressure to escape more easily. Therefore, the difference in behaviour

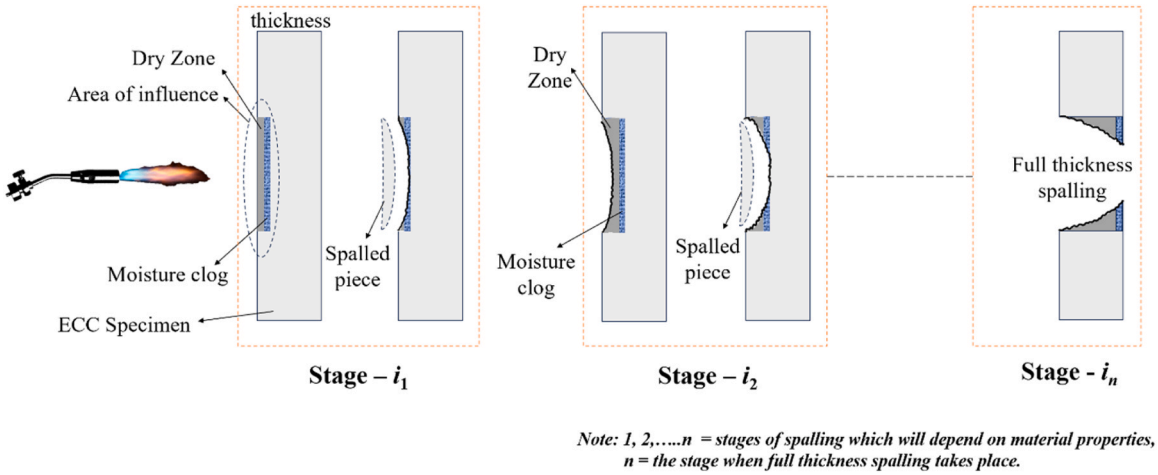

Fig. 24. Different stages of spalling during 1-D exposure test.

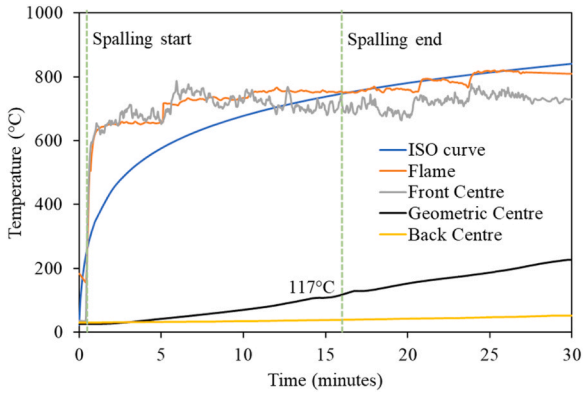

Fig. 25. Temperature profile of PP0.5PE1.25BF0.75 mix 300 × 300 × 50 panel specimens during 1-D exposure test.

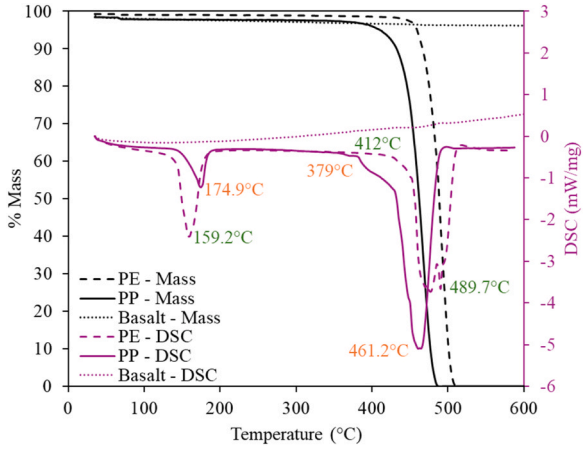

Fig. 26. Thermogravimetric (TG) and differential scanning calorimetry (DSC) curves of different fibres used in the study.

might have been primarily due to the difference in type and dosage of fibres.

Under 1-D fire exposure, spalling occurred in successive layers (stages), potentially due to moisture clog formation as shown in Fig. 24. In mixes without fibres, the matrix is homogenous, and the voids and permeability are more uniform, meaning the behaviour is mainly dependent on the density of the microstructure. However, in fibre-reinforced mixes, the introduction of fibres creates non-homogeneity in the material, which affects the ability of the specimen to resist spalling. Depending on their properties and distribution, fibres either hinder or assist pore pressure dissipation. Fig. 25 further illustrates temperature distribution in one of the specimens (mix PP0.5PE1.25BF0.75), showing that even at the end of the spalling period, the temperature of the core only reached 120°C, while the backside was around 50°C. Since the melting points of both PE and PP fibres are higher than these temperatures, melting alone was unlikely to fully prevent spalling. Instead, factors such as fibre distribution, melt viscosity, thermal expansion, and fibre-matrix bonding were crucial as described below.

6.1. *Fibre-matrix bonding and thermal expansion*

Fibre-matrix bonding and the thermal expansion of fibres significantly influence spalling behaviour, particularly under 1-D heating. PP fibres bond weakly with the cementitious matrix, and PE fibres also have poorer bonding compared to basalt fibres [37]. This weak adhesion can create spaces that facilitate water or vapour transport (pressure-induced tangential space or PITS), aiding pore pressure dissipation [38]. In the mix PP0PE1.25BF0.75, there were two fundamental issues: PE fibres did not form a continuous network, hindering pore pressure dissipation, and the basalt fibres further obstructed this network due to their strong bonding with the matrix. However, increasing the PE fibre length to 18 mm significantly improved behaviour, likely because longer PE fibres were able to form a more effective interconnected network for pore pressure dissipation through PITS. Additionally, the thermal expansion coefficients of the fibres (before melting) played a role. Generally, PP fibres have a higher thermal expansion coefficient than PE fibres, while basalt fibres are thermally stable below 200°C. As the temperature rises, the mismatch in thermal expansion between the fibres and the matrix can cause more cracking [39], which allows polymer fibres to aid in pore pressure dissipation even without melting. This explains the better spalling resistance observed in mixes PP0.3PE1.25BF0.75 and PP0.5PE1.25BF0.75.

6.2. *Fibre melting, vaporisation and melt viscosity*

For 3-D exposure, where heating occurs from all directions, fibre melting can contribute to the formation of a more continuous network of voids for vapour release. However, even if certain parts of the specimen exceed the melting point of polymer fibres, factors such as melt viscosity and vaporisation point are crucial in determining their effectiveness. For instance, PE fibres have a lower melting point than PP fibres (PE: 159°C vs PP: 175°C, as shown in Fig. 26), which suggests that all specimens, including those with hybrid PE-basalt fibres, should exhibit better

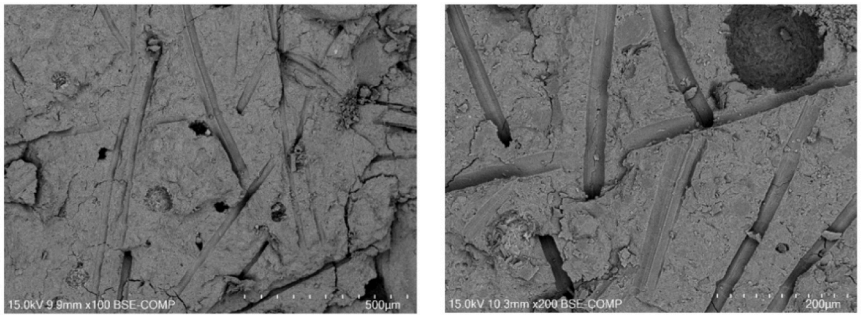

Network of melted polymer fibre channels - Mix PP0.5PE2BF0

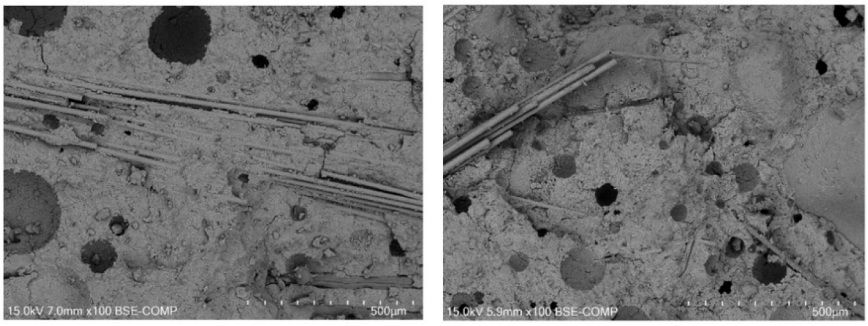

Agglomeration of basalt fibres - Mix PP0PE1.25BF0.75

Fig. 27. Network of melted polymer fibres and basalt fibres after 1-D exposure test.

spalling resistance if fibre melting was the primary factor. However, PE fibres have significantly higher melt viscosity [40] and vaporisation points (PE: 412–489°C, PP: 379–461°C), which limits their effectiveness in comparison to PP fibres. Therefore, fibre melting alone is not the sole mechanism responsible for spalling resistance—melt viscosity and vaporisation point must also be taken into account. Basalt fibres, with their very high melting points, do not contribute to this mechanism. This was also the reason of better spalling resistance of PP0PE2BF0 and PP0.5PE2BF0 under both 1-D and 3-D exposure.

6.3. *Fibre distribution*

The distribution of fibres also plays a critical role in spalling resistance. While the overall flow can be controlled, precise fibre distribution is difficult to achieve. PP and PE fibres are generally more uniformly distributed, helping to create a more interconnected network. However, basalt fibres are less effective at forming this network due to their agglomeration (as seen in Fig. 27), which may explain why the inclusion of 0.75 % basalt fibre did not enhance spalling resistance.

Overall, the mechanism involves the buildup of pressure and associated spalling, which can only be resisted if a network is formed inside the matrix to transfer the vapours. This may also explain the better spalling resistance observed in smaller-sized or thinner specimens due to the shorter required network. Under 1-D exposure, this network is more likely to form when the fibres do not strongly adhere to the matrix, making PP and PE fibres effective in that order. Additional matrix defects and the thermal expansion of the fibres may further aid this process. Since both PP and PE fibres have higher thermal expansion coefficients (PP > PE), they help dissipate pore pressure even without melting and their melting plays a less significant role because only a limited area reaches high temperature. However, fibre melting may be beneficial under 3-D fire exposure. Nonetheless, it should be noted that fibre melting should be considered along with melt viscosity and vaporisation point. The lower melt viscosity of PP fibre makes it more advantageous than PE fibre. Finally, fibre distribution is also crucial as fibres that form clogged networks can hinder the dissipation mechanism. Additionally, smaller specimens (50 ×50 mm, 100 ×100 mm) may not effectively represent spalling sensitivity, as the network of interconnected channels may be more effective due to the shorter path. Therefore, spalling testing should preferably be conducted on larger specimens, such as 300 × 300 mm.

7. Conclusion

This study systematically analysed the performance of single and hybrid PE fibre-reinforced ECC under fire exposure. The composites were examined at both the material and structural scales to understand its residual mechanical performance and spalling resistance, as well as to gain further insights into the underlying mechanism. The paper also developed a 1-D spalling test, which was used for spalling test, and the test results were compared with those from the 3-D exposure tests. Based on the result analyses and findings, the following conclusions can be drawn:

- The developed 1-D blow torch test, with standardized parameters (nozzle diameter, specimen size, and distance), was demonstrated to be a simple but reliable and cost-effective method for assessing spalling resistance. The obtained test results closely correlated with those from 3-D tests conducted in this study.
- Material-scale testing demonstrated the superior performance of PE-ECC with 2 % PE fibre, achieving superior compressive and tensile strength both at room and elevated temperatures. Addition of basalt fibres as replacement to PE fibres further enhanced compressive strength and tensile strength retention at elevated temperatures but did not improve strain-softening behaviour, as failure occurred in a single crack mode.
- The 300 × 300 × 50 mm panel with 2 % PE fibre content exhibited a maximum spalling depth of 9 mm under 1-D exposure and showed minor surface spalling under 3-D exposure. However, the hybrid combination of 12 mm 1.25 % PE fibre and 12 mm 0.75 % basalt

fibre did not provide adequate spalling resistance, as specimens spalled to full thickness under 1-D exposure. Improved spalling resistance was achieved by increasing the PE fibre length to 18 mm or by adding 0.3 % PP fibre. This indicates that PE fibres were crucial in reducing spalling, while basalt fibres showed limited effectiveness. This was likely due to their strong bonding with the matrix, poor distribution, and high thermal stability, all of which hindered the formation of effective vapour-release channels.

- Spalling resistance was found better for panel specimens with lower thickness (20 mm) and smaller surface area (50 ×50, 100 ×100, 200 ×200), emphasizing the importance of specimen size in accurately capturing spalling sensitivity. For accurate assessment, the 1-D test with 300 × 300 × 50 mm specimens should be preferred.
- In PE fibre-reinforced ECC, fibre melting alone is not sufficient for enhancing performance. Key factors influencing spalling resistance include fibre distribution, melt viscosity, and vaporisation point. Under 1-D exposure, fibre distribution is crucial for generating PITS, whereas under 3-D exposure, the melting characteristics of fibres, such as melt viscosity and vaporisation point, play a more significant role.

CRediT authorship contribution statement

S. Rawat: Writing – original draft, Visualization, Methodology, Investigation, Formal analysis, Conceptualization, Data curation. **Lihai Zhang:** Methodology, Writing – review & editing, Supervision, Funding acquisition. **Y. X. Zhang:** Methodology, Writing – review & editing, Supervision, Funding acquisition, Project administration.

Declaration of Competing Interest

The authors declare that they have no known competing financial interests or personal relationships that could have appeared to influence the work reported in this paper

Acknowledgement

This research was funded by the Australian Government through Australian Research Council Discovery Project (DP220103043). The authors would also like to acknowledge the Civil and Structural Engineering labs and Advanced Materials Characterisation Facility (AMCF) of Western Sydney University for access to its instrumentation and staff.

Data availability

Data will be made available on request.

References

[1] Wang YS, Zhou H, Wu JY. Hybrid fire collapse simulation of reinforced concrete structures under localized fires. Eng Struct 2023;292:116525.
[2] Liu JC, Tan KH, Yao Y. A new perspective on nature of fire-induced spalling in concrete. Constr Build Mater 2018;184:581–90.
[3] Rawat S, Lee CK, Zhang YX. Performance of fibre-reinforced cementitious composites at elevated temperatures: A review. Constr Build Mater 2021;292:123382.
[4] Missemer L, Ouedraogo E, Malecot Y, Clergue C, Rogat D. Fire spalling of ultra-high-performance concrete: From a global analysis to microstructure investigations. Cem Concr Res 2019;115:207–19.
[5] Li VC. Engineered cementitious composites (ECC): bendable concrete for sustainable and resilient infrastructure. Springer; 2019.
[6] Liu JC, Tan KH. Fire resistance of ultra-high performance strain hardening cementitious composite: Residual mechanical properties and spalling resistance. Cem Concr Compos 2018;89:62–75.
[7] Zhang D, Liu Y, Tan KH. Spalling resistance and mechanical properties of strain-hardening ultra-high performance concrete at elevated temperature. Constr Build Mater 2021;266:120961.
[8] Zhang Z, Li Z, He J, Qian S, Shi X. Recycled mask polypropylene microfibers benefit tensile properties and prevent thermally induced spalling of high-strength engineered cementitious composite (HS-ECC). J Clean Prod 2024;457:142476.
[9] Rawat S, Zhang YX, Lee CK. Spalling Resistance of Hybrid Polyethylene and Steel Fiber-Reinforced High-Strength Engineered Cementitious Composite. In: Duan W, Zhang L, Shah SP, editors. Nanotechnology in Construction for Circular Economy. NICOM 2022. Lecture Notes in Civil Engineering, 356. Singapore: Springer; 2023. https://doi.org/10.1007/978-981-99-3330-3_33.
[10] Li Y, Yang EH, Tan KH. Flexural behavior of ultra-high performance hybrid fiber reinforced concrete at the ambient and elevated temperature. Constr Build Mater 2020;250:118487.
[11] Rawat S, Zhang YX, Fanna DJ, Lee CK. Development of sustainable engineered cementitious composite with enhanced compressive performance at elevated temperatures using high volume GGBFS. J Clean Prod 2024;451:142011.
[12] Zhang X, Lyu X, Zhang X, Lou C. Effect of high temperature on mechanical properties of polyethylene fibre-calcium carbonate whisker engineered cementitious composites. Dev Built Environ 2024;18:100462.
[13] Cai Z, Liu F, Yu J, Yu K, Tian L. Development of ultra-high ductility engineered cementitious composites as a novel and resilient fireproof coating. Constr Build Mater 2021;288:123090.
[14] Cai ZW, Yu JT, Tian LK, Liu FC, Yu KQ. Fire resistance of post-earthquake steel beams insulated with a novel fire-resistive coating-FR-ECC. Eng Struct 2021;246:112887.
[15] Xiong Y, Lin K, Wu D, Ling Y, Tesfamariam S. The role of a novel coating of SFRCR-ECC in enhancing the fire performance of CFST columns: Development, characteristic and ISO-834 standard fire test. Eng Struct 2023;294:116629.
[16] Rawat S, Zhang YX, Lee CK. Effect of specimen size and shape on the compressive performance of high strength engineered cementitious composites at elevated temperatures. Innov Infrastruct Solut 2024;9(8):317.
[17] Li VC, Kanda T. Innovations forum: engineered cementitious composites for structural applications. J Mater Civ Eng 1998;10(2):66–9.
[18] Rokugo K, Kanda T, Kanakubo T, Fukuyama H, Uchida Y, Suwada H, Slowik V. Strain Hardening Cement Composites: Structural Design and Performance: State-of-the-Art Report of the RILEM Technical Committee 208-HFC, SC3. Berlin/Heidelberg, Germany: Springer; 2013.
[19] Rawat S, Vongsvivut J, Zhang L, Zhang YX. Mechanical performance and microstructure evolution of MgO-doped high volume GGBFS-based engineered cementitious composites at room and elevated temperatures. J Build Eng 2024;98:111437.
[20] Du P, Yang Y, Tan KH. Fire behaviour and design of hybrid fibre reinforced high-performance concrete columns subjected to uniaxial bending. Eng Struct 2022;251:113425.
[21] Shen S, Zhuang J, Yang Y, Dong S. Mechanical performances and micro-level properties of basalt and PVA fiber reinforced engineered cementitious composite after high temperatures exposure. J Build Eng 2023;79:107870.
[22] Rawat S, Lee CK, Zhang YX. Green engineered cementitious composites with enhanced tensile and flexural properties at elevated temperatures. Clean Mater 2024;12:100240.
[23] Ahmad F, Rawat S, Yang RC, Zhang L, Guo Y, Fanna DJ, Zhang YX. Effect of hybrid fibres on mechanical behaviour of magnesium oxychloride cement-based composites. Constr Build Mater 2024;424:135937.
[24] Zhang D, Zhang Y, Dasari A, Tan KH, Weng Y. Effect of spatial distribution of polymer fibers on preventing spalling of UHPC at high temperatures. Cem Concr Res 2021;140:106281.
[25] Maluk C, Bisby L, Terrasi GP. Effects of polypropylene fibre type and dose on the propensity for heat-induced concrete spalling. Eng Struct 2017;141:584–95.
[26] Banerji S, Kodur V, Solhmirzaei R. Experimental behavior of ultra high performance fiber reinforced concrete beams under fire conditions. Eng Struct 2020;208:110316.
[27] Song C, Zhang G, Lu Z, Li X, Zhao X. Fire resistance tests on polypropylene-fiber-reinforced prestressed concrete box bridge girders. Eng Struct 2023;282:115800.
[28] Rawat S, Saliba P, Estephan PC, Ahmad F, Zhang Y. Mechanical performance of hybrid fibre reinforced magnesium oxychloride cement-based composites at ambient and elevated temperature. Buildings 2024;14(1):270.
[29] Pan Z, Wu C, Liu J, Wang W, Liu J. Study on mechanical properties of cost-effective polyvinyl alcohol engineered cementitious composites (PVA-ECC). Constr Build Mater 2015;78:397–404.
[30] Zhu M, Chen B, Wu M, Han J. Effects of different mixing ratio parameters on mechanical properties of cost-effective green engineered cementitious composites (ECC). Constr Build Mater 2022;328:127093.
[31] Khan MKI, Zhang YX, Lee CK. Mechanical properties of high-strength steel–polyvinyl alcohol hybrid fibre engineered cementitious composites. J Struct Integr Maint 2021;6(1):47–57.
[32] Helal KA, Tahwia AM, Youssf O. Performance of eco-friendly ECC made of pre-treated crumb rubber and waste quarry dust. J Build Eng 2024;97:110820.
[33] Helal KA, Tahwia AM, Youssf O. Assessment of the efficiency of hybrid basalt fibre sustainable ECC incorporating industrial waste materials. Constr Build Mater 2025;461:139933.
[34] Shoji D, He Z, Zhang D, Li VC. The greening of engineered cementitious composites (ECC): a review. Constr Build Mater 2022;327:126701.
[35] Mugume RB, Horiguchi T. Prediction of spalling in fibre-reinforced high strength concrete at elevated temperatures. Mater Struct 2014;47:591–604.
[36] Lo Monte, F., Felicetti, R., Meda, A., & Bortolussi, A. (2017). Influence of the test method in the assessment of concrete sensitivity to explosive spalling. In Proceedings from the 5th International Workshop on Concrete Spalling, Borås, Sweden, 12-13 October 2017 SP Report: 2017: 43 (pp. 289-300). RISE Research Institutes of Sweden.

[37] Xu M, Song S, Feng L, Zhou J, Li H, Li VC. Development of basalt fiber engineered cementitious composites and its mechanical properties. Constr Build Mater 2021; 266:121173.
[38] Khoury GA. Polypropylene fibres in heated concrete. Part 2: pressure relief mechanisms and modelling criteria. Mag Concr Res 2008;60(3):189–204.
[39] Zhang D, Tan KH. Effect of various polymer fibers on spalling mitigation of ultra-high performance concrete at high temperature. Cem Concr Compos 2020;114: 103815.
[40] Knack, I. (2011). The use of PP fibers in tunnel construction to avoid explosive concrete spalling in case of fire. New test results for the clarification of the mode of action. In Proceedings of the 2nd International RILEM Workshop on Concrete Spalling due to Fire Exposure, Delft, The Netherlands (pp. 5-7).